Energy-Efficient Hybrid Beamforming for Multi-Layer RIS-Assisted Secure Integrated Terrestrial-Aerial Network

Yifu Sun, Kang An, Yonggang Zhu, Gan Zheng, *Fellow, IEEE,* Kai-Kit Wong, *Fellow, IEEE,* Symeon Chatzinotas, *Senior Member, IEEE*, and Dongfang Guan, *Senior Member, IEEE,* and Derrick Wing Kwan Ng, *Fellow, IEEE*

Abstract—The integration of aerial platforms to provide ubiquitous coverage and connectivity for densely deployed terrestrial networks is expected to be a reality in emerging sixth-generation networks. Energy-effifficient design and secure transmission are two crucial issues for integrated terrestrial-aerial networks. With this focus, due to the potential of RIS in substantially saving power consumption and boosting the security of private information by enabling a smart radio environment, this paper investigates the energy-efficient hybrid beamforming for multi-layer reconfigurable intelligent surface (RIS)-assisted secure integrated terrestrial-aerial network for defending against simultaneous jamming and eavesdropping attacks. Specifically, with the available of angular information based imperfect channel state information (CSI), we propose a framework for the joint optimization of user's received precoder, terrestrial BS's and HAP's digital precoder, and multi-layer RIS analog precoder to maximize the system energy efficiency (EE) performance. For the design of received precoder, a heuristic beamforming scheme is proposed to convert the worst-case problem into a min-max one such that a closed-form solution is derived. For the design of digital precoder, we propose an iterative sequential convex approximation approach via capitalizing the auxiliary variables and first-order Taylor series expansion. Finally, a monotonic vertex-update algorithm with penalty convex concave procedure is proposed to obtain analog precoder with low computational complexity. Numerical results show the superiority and effectiveness of proposed optimization framework and architecture.

Index Terms—Reconfigurable intelligent surface, secure integrated terrestrial-aerial network, energy-efficient hybrid beamforming, imperfect angular information.

I. INTRODUCTION

WITH the increasing demand for sustainable and flexible connectivity in either semi-urban/rural areas or disaster rescue, monitoring/surveillance scenarios, the usage of aerial

Y. Sun, K. An, Y. Zhu, and D. Guan are with National University of Defense Technology, China (Email: sunyifu.nudt,ankang89@nudt.edu.cn; zhumaka1982@163.com).

G. Zheng is with the Wolfson School of Mechanical, Electrical and Manufacturing Engineering, Loughborough University, Loughborough LE11 3TU, U.K. (e-mail: g.zheng@lboro.ac.uk).

K.-K Wong is with the Department of Electronic and Electrical Engineering, University College London, London WC1E 7JE, U.K. (e-mail: kai-kit.wong@ucl.ac.uk).

D. W. K. Ng is with the School of Electrical Engineering and Telecommunications, University of New South Wales, Sydney, NSW 2025, Australia (e-mail: w.k.ng@unsw.edu.au).

S. Chatzinotas is with Interdisciplinary Centre for Security, Reliability and Trust, University of Luxembourg, Luxembourg, L-1855, Luxembourg (e-mail: symeon.chatzinotas@uni.lu).

platforms for enhancing the network coverage and, thereby, the service availability of terrestrial networks, has received substantial attentions [1]. This vision has been proposed by the 3rd Generation Partnership Project (3GPP) for the operation of New Radio in non-terrestrial networks, which basically consists of high-altitude platform stations (HAPSs), unmanned aerial vehicles and satellite deployments due to their intrinsic features such as longer operating time, small footprinting and wide coverage area [2]. To exploit the advantages of both terrestrial and HAP networks, the framework of integrated terrestrial-aerial networks (ITAN) have been proposed for future sixth-generation (6G) communication networks [3]–[5].

Due to the inherent openness and broadcast nature of the wireless medium, ITAN is vulnerable to security breaches, including the active jamming attacks for interrupting transmissions and the passive eavesdropping attacks for data interception. Traditionally, frequency hopping (FH) [6] and spatial anti-jamming method [7] have been extensively adopted to tackle the jamming attacks in wireless networks, where the former method can turn the current working frequencies of cooperative parties to be orthogonal to the jamming signals and the later method boosts desired signal and nullify jamming signal at the intended recipient (see [6], [7] and reference therein). However, FH consumes extra spectrum resources, and the implementation of spatial beamforming with multiple antennas incur high hardware cost. As for combating eavesdropping attacks, the existing works in the literature utilized the intrinsic randomness of the noise and the characteristics of wireless channel to limit the eavesdroppers achievable rate, which includes multi-antenna beamforming [8], [9], artificial noise (AN) [10], and cooperative jamming [11]. Particularly, the multiple-antenna techniques use spatial selectivity to improve the stealthiness of wireless channel through directional transmission, while AN tries to avert the negative impact of jamming signals on legitimate channels. Besides, cooperative relaying scheme relies on cooperation from the intermediate node to facilitate the channel difference between the legitimate users and eavesdroppers. Nevertheless, the implementation of AN and cooperative jamming incurs additional power consumption, and cooperative jamming needs to cooperate with additional nodes, which constitutes an inevitable burden from the perspective of deployment scalability.

In addition, due to the huge power consumption of base stations, energy efficiency (EE) has been regarded as an

important metric for the future communication networks in terms of economic and ecological aspects [12]. In this regard, the authors in [12] jointly optimized the transmit beamforming and AN covariance matrix to maximize the global EE in a multiple-input-single-output (MISO) system. In [13], the authors studied the EE maximization problem for a ITAN, and proposed two array signal processing methods based on the Dinkelbach's transformation to obtain approximate solutions. However, due to the huge number of active antennas required by transmit beamforming, the abovementioned schemes have extreme high hardware power consumption and hence EE is very low. Although the alternative hybrid beamforming has been proposed to address the issue, the analog network still consumes high hardware power and thus has low EE [14].

To address the abovementioned shortcomings, a spectrum and energy-efficient paradigm, called reconfigurable intelligent surface (RIS), is utilized to enhance the security and improve the EE of ITAN in this paper. Specifically, RIS is a metasurface comprising of many low-cost passive units, where each unit can impose a phase shift and/or amplitude to the incident signal, thus reflecting the electromagnetic (EM) wave to the desired direction [15]. Current state-of-the-art for RIS-assisted communication system can be generally divided into two aspects: RIS as a passive reflector for reconfiguring the EM propagation environment [15] and RIS acts as an active transceiver for analog beamforming at low hardware cost and power consumption [16]. In the existing literatures, RIS-based passive reflector has been widely investigated to improve network capacity and EE [17], [18], enhance physical layer security [19]–[21], and improve anti-jamming performance [21]. In our previous work [21], RIS was first utilized to enhance secure transmission against both jamming and eavesdropping attacks in the cellular networks, where the achievable rate was maximized by joint optimizing the active transmit beamforming at the BS and the passive reflecting beamforming at the RIS under secrecy constraint and imperfect channel state information (CSI). However, RIS-based passive reflector can also reflect the jamming signal such that the enhancement of desired signal and the suppression of the jamming signal cannot be perfectly balanced. After all, RIS-based passive reflector may suffers from the "double fading" effect, namely, the large-scale fading first in the transmitter-RIS link and then again in the RIS-receiver link. Thus, this paper turns to the second aspect: RIS-assisted transmitter. The key advantage of the RIS-assisted transmitter is that it requires much less power and cost compared with the conventional transmitter, since it eliminates the need for active phase shifter, power amplifiers, and complicated RF chains [14]. The authors in [14] first proposed two novel RIS-aided transmitter architectures for single-user massive MIMO system, but the non-uniform feed's power distribution on RIS leads to performance degradation. To address this issue, the authors in [22] proposed multi-layer RIS-aided transmitter to make the power distribution more uniform, and thus both phase and amplitude of the signal penetrating multi-layer RIS-aided transmitter can also be partially controlled so that the performance is enhanced. However, the aforementioned works on design and implementation of RIS-based transmitter architectures are not applicable to the het-

erogeneous multi-user systems. Moreover, the EE optimization under the secure transmission perspective remains an open issue, which requires deep investigation, particularly in the presence of CSI imperfection.

Motivated by the above observations, we investigate the EE optimization problem for multi-layer RIS-assisted secure ITAN in the presence of imperfect CSI. Specifically, the main contributions of this paper are summarized as follows:

- An architecture of RIS-aided secure ITAN against simultaneous jamming and eavesdropping attacks is first proposed, where a multi-layer RIS-assisted transmitter is adopted at the BS to secure downlink transmission and facilitate the employment of large-scale array[1], which can break the dimensionality limit of beamforming design and reduces the hardware cost of ITAN. Besides, under the imperfect angular CSI of both jamming and wiretap channel and no knowledge of the jammer's transmit beamforming, a worst-case optimization problem is formulated to maximize the EE by jointly designing the received precoder at users, the digitial precoder at BS and HAP, and the analog precoder at RIS, while satisfying the desired target rate and wiretap rate requirements.[2]

- Since the formulated EE maximization problem is non-convex, an optimization framework is proposed to solve it. Specifically, we first express the continuous angular uncertainty as the weighted combination of discrete elements, and then we convert the worst-case problem into min-max one such that a heuristic beamforming scheme is proposed to identify the closed-form solutions of received precoder. Then, we propose a sequential convex approximation (SCA) method to solve the worst-case EE maximization problem for obtaining the digital precoder. Finally, a novel monotonic vertex-update (MVU) algorithm combining with penalty convex concave procedure (P-CCP) is proposed to achieve analog precoder.

- It is worth-mentioning that the proposed optimization framework can be also applicable to the achievable rate maximization (as well as secrecy EE maximization) problem in the RIS-aided downlink system, and the same optimization problem with typical transmitter architectures. Numerical results clearly demonstrate the potential performance gains reaped by our proprosed optimization framework and architecture against various existing benchmark approaches and architectures.

The remainder of this work is organized as follows. The system model and the problem formulation are presented in Section II. In Section III, the heuristic beamforming method, SCA method, and MVU scheme, including the discretization method and P-CCP, are proposed. Numerical results are pro-

---

[1]In the traditional antenna arrays, numerous radio-frequency (RF) components, like RF chains in the fully digital architecture and phased arrays in the hybrid architecture, is required, which leads to high hardware cost and excessive power consumption at BS.

[2]To the best of our knowledge, the EE maximization problem with a multi-layer RIS-assisted hybrid array is addressed for the first time in this paper whereas existing works on TAIN focused on different performance criteria with different array architectures, e.g. [8] aimed at power minimization with all digital array, while [23] focused on secrecy EE maximization with conventional hybrid array.
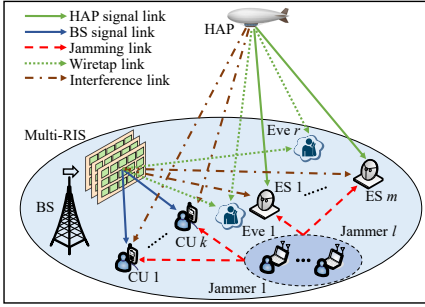
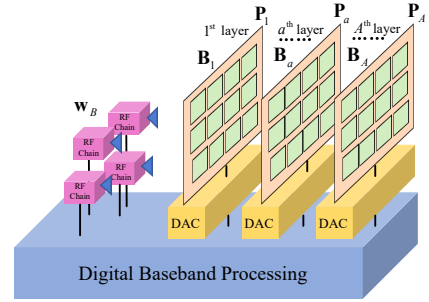Fig. 1: System model of the considered secure ITAN.

Fig. 2: System model of multi-layer RIS-assisted transmitter.

(a) First layer.

(b) Second layer.

Fig. 3: A simulation result of power distributions of the signal received on different layers when $N_R = 8 \times 8$.

vided in Section IV. We conclude this paper in Section V.

II. SYSTEM MODEL AND PROBLEM FORMULATION

A. System Model

Fig. 1 illustrates the system model of considered secure ITAN, where BS equipped with the multi-layer RIS-assisted transmitter, tries to establish the reliable links with K cellular users (CUs) using broadcast communications, while the HAP acts as a fixed aerial base station to serve M earth stations (ESs) using unicast communications as in [5] and [9] [3]. In addition, there exists both L active jammers for disrupting legitimate transmissions and R passive eavesdroppers (Eves) for unauthorized data interception. It is assumed that the BS is equipped with N_{RF} feeds, and the multi-layer RIS is composed of A layers having $N_{R,a}$ units on the a-th layer. Furthermore, we assume that the HAP and the l-th jammers apply uniform planar arrays (UPA) with N_H units and $N_{J,l}$ antennas, respectively. To nullify the jamming signals and eliminate the interference from the other network, the k-th CU and m-th ES are equipped with $N_{C,k}$ and $N_{S,m}$ UPA antennas, respectively. Without loss of generality, we set $N_{R,a} = N_R, \forall a \in [A]$, $N_{J,l} = N_J, \forall l \in [L]$, $N_{C,k} = N_C, \forall k \in [K]$, and $N_{S,m} = N_S, \forall m \in [M]$. Since the eavesdroppers wishes to intercept the data form different directions, we assume it use omnidirectional single-antenna.

B. Multi-Layer RIS-Assisted Transmitter Architecture

Conventional MIMO systems have three typical transmitter architectures, namely, the full-digital precoding architecture, the fully-connected hybrid precoding architecture, and sub-connected hybrid precoding architecture, which has been illustrated in Fig. 1 (a)-(c) in [14]. Clearly, the RF chains required by the full-digital precoding architecture are equal to the number of antennas, and thus obtains better spectral efficiency with prohibitively RF power consumption and computational burden. Alternatively, the fully-connected hybrid precoding architecture is exploited to achieve a satisfactory cost-performance trade-off due to the use of fewer RF chains.

[3]The multi-layer RIS-assisted transmitter can be also deployed at the HAP using a similar structure, which can also achieve the structural benefits discussed, and the optimization algorithms proposed in Section III can be also applied to it. Thus, the work that apply the multi-layer structure at both the BS and the HAP is omitted in this paper for simplicity.
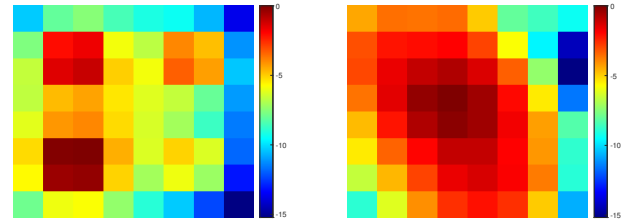
However, since each RF chains of fully-connected scheme are connected to all the phase-array antennas, the number of required phase shifters is proportional to the number of antennas as well as the number of RF chains, which makes the fully-connected scheme also not scalable and energy-hungry. To address this issue, the sub-connected scheme, whose RF chains is connected to a part of antennas, is proposed to eliminate the need for RF combiners and phase shifters. Nevertheless, the analog network's cost of sub-connected scheme is still very high for large numbers of antennas [14]. With this regard, in the proposed RIS-assisted transmitter architecture, the low-cost and energy-efficient RIS is utilized to replace the energy-hungry phased array in the conventional hybrid architecture to perform the analog beamforming, see Fig. 2. Specifically, the RIS is vertically deployed in front of the feeds to serve as both the analog networks and transmit antennas. However, as illustrated in Fig. 3 (a), the power distribution from the feeds to the RIS is non-uniform. In particular, the central elements are assigned most of the power, whereas the non-central units has a limited contribution, which leads to the performance degradation. To overcome this shortcoming, the multi-layer RIS are vertically stacked in front of the feeds to form the energy-efficient transmitter, with a flexible gap between adjacent vertical layers [22]. As such, as shown in Fig. 3 (b), the power distribution is transformed into a more balanced power pattern in the second layer. Note that the key advantages of the multi-layer RIS-assisted transmitter is two-fold. Firstly, the feed mechanism of proposed architectures is referred to as space feeding mechanism, while that of conventional hybrid architecture is through the analog network which can incur a

TABLE I: Description of the signal model parameters

Parameter	Definition
$\mathbf{B}_1$	channel vector (CV) between feeds and 1st layer
$\mathbf{B}_a$	CV between $(a-1)$-th layer and a-th layer
$\mathbf{H}_{C,k}$ / $\mathbf{H}_{S,m}$	CV between BS and k-th CU / m-th ES
$\mathbf{F}_{C,k}$ / $\mathbf{F}_{S,m}$	CV between HAP and k-th CU / m-th ES
$\mathbf{Z}_{C,lk}$ / $\mathbf{Z}_{S,lm}$	CV between l-th jammer and k-th CU / m-th ES
$\mathbf{h}_{E,r}$ / $\mathbf{f}_{E,r}$	CV between BS / HAP and r-th Eve
$\sigma_{C,k}^2$ / $\sigma_{S,m}^2$ / $\sigma_{E,r}^2$	noise variance at k-th CU / m-th ES / r-th Eve

high hardware cost. Secondly, according to **_Lemma 1_** in [22], as compared to the single-layer RIS-assisted transmitter, the power distribution on RIS is more uniform, and the amplitude of the signal penetrating multi-layer RIS-assisted transmitter can be also partially controlled, which brings about a new degree of freedom (DoF) for beamforming design that can be beneficially exploited for performance enhancement. Thus, the abovementioned advantages confirms the fact that the multi-layer RIS-assisted transmitter is inherently more energy-efficient [14], [22], [24], [25].

C. Signal Transmission Model

Denote $x_{H,m}$ as the desired information signal transmitted by the HAP to the m-th ES, which satisfies $\mathrm{E}\left\{|x_{H,m}|^2\right\} = 1$. Prior to transmission, the signal is weighted by a digitial beamforming vector $\mathbf{w}_{H,m} \in \mathbb{C}^{N_H \times 1}$. Meanwhile, the BS transmits a composite normalized signal x_B, i.e., $\mathrm{E}\left\{|x_B|^2\right\} = 1$, to the CUs in its coverage area. As analyzed in Section II-A, to reduce the system cost and complexity induced by a large number of RF chains, the BS employs the multi-layer RIS-assisted transmitter to perform hybrid analog-digital beamforming, where $\mathbf{P}_a = \mathrm{diag}\left\{\mathbf{p}_a\right\} = \mathrm{diag}\left\{e^{j\theta_{a,1}}, \cdots, e^{j\theta_{a,N_R}}\right\} \in \mathbb{C}^{N_R \times N_R}$ denotes the a-th RIS-aided analog precoder and $\mathbf{w}_B \in \mathbb{C}^{N_{RF} \times 1}$ denotes the digital beamforming vector for x_B. Here, the symbol $e^{j\theta_{a,n}} \in [0, 2\pi)$ denotes the phase shift of the n-th RIS unit on the a-th layer. In addition, the k-th CU and m-th ES employ the baseband digital processing matrix $\mathbf{v}_{C,k} \in \mathbb{C}^{N_C \times 1}$, $\mathbf{v}_{S,m} \in \mathbb{C}^{N_S \times 1}$ to nullify the jamming signals and balance the interference, respectively. Other system model parameters are listed in Table I. As such, the received signals at the k-th CU, m-th ES, and r-th eavesdropper are, respectively, expressed as

$$y_{C,k} = \mathbf{v}_{C,k}^H \left(\mathbf{H}_{C,k} \boldsymbol{\Omega}_{(1,A)} \mathbf{w}_B x_B + \sum_{m=1}^{M} \mathbf{F}_{C,k} \mathbf{w}_{H,m} x_{H,m} \right.$$
$$\left. + \sum_{l=1}^{L} \mathbf{Z}_{C,lk} \mathbf{w}_{J,l} + \mathbf{n}_{C,k} \right), \quad (1)$$

$$y_{S,m} = \mathbf{v}_{S,m}^H \left(\mathbf{F}_{S,m} \mathbf{w}_{H,m} x_{H,m} + \sum_{i=1,i\neq m}^{M} \mathbf{F}_{S,m} \mathbf{w}_{H,i} x_{H,i} \right.$$
$$\left. + \mathbf{H}_{S,m} \boldsymbol{\Omega}_{(1,A)} \mathbf{w}_B x_B + \sum_{l=1}^{L} \mathbf{Z}_{S,lm} \mathbf{w}_{J,l} + \mathbf{n}_{S,m} \right), \quad (2)$$

$$y_{E,r} = \mathbf{h}_{E,r}^H \boldsymbol{\Omega}_{(1,A)} \mathbf{w}_B x_B + \sum_{m=1}^{M} \mathbf{f}_{E,r}^H \mathbf{w}_{H,m} x_{H,m} + n_{E,r}, \quad (3)$$

where $\mathbf{n}_{C,k} \sim \mathcal{CN}(0, \sigma_{C,k}^2 \mathbf{I}_{N_C})$, $\mathbf{n}_{S,m} \sim \mathcal{CN}(0, \sigma_{S,m}^2 \mathbf{I}_{N_S})$, and $n_{E,r} \sim \mathcal{CN}(0, \sigma_{E,r}^2)$ denote the additive white Gaussian noise (AWGN) for k-th CU, m-th ES, and r-th Eve, respectively. For notational simplicity, we define

$$\boldsymbol{\Omega}_{(u,v)} = \begin{cases} \prod_{a=u}^{v} \mathbf{P}_a \mathbf{B}_a, u, v \in [A], \\ \mathbf{I}_{N_R}, u = A, v = A+1, \\ \mathbf{I}_{N_{RF}}, u = 0, v = 1. \end{cases} \quad (4)$$

The achievable rate of k-th CU and m-th ES are given by

$$R_{C,k} = \log_2\left(1 + \left|\mathbf{v}_{C,k}^H \mathbf{H}_{C,k} \boldsymbol{\Omega}_{(1,A)} \mathbf{w}_B\right|^2 \Big/ \beta_{C,k}\right), \quad (5)$$

$$R_{S,m} = \log_2\left(1 + \left|\mathbf{v}_{S,m}^H \mathbf{F}_{S,m} \mathbf{w}_{H,m}\right|^2 \Big/ \beta_{S,m}\right), \quad (6)$$

where

$$\beta_{C,k} = \sum_{m=1}^{M}\left|\mathbf{v}_{C,k}^H \mathbf{F}_{C,k} \mathbf{w}_{H,m}\right|^2 + \sum_{l=1}^{L}\left|\mathbf{v}_{C,k}^H \mathbf{Z}_{C,lk} \mathbf{w}_{J,l}\right|^2 + \left|\mathbf{v}_{C,k}^H \mathbf{n}_{C,k}\right|^2,$$

$$\beta_{S,m} = \sum_{i=1,i\neq m}^{M} \left|\mathbf{v}_{S,m}^H \mathbf{F}_{S,m} \mathbf{w}_{H,i}\right|^2 + \left|\mathbf{v}_{S,m}^H \mathbf{H}_{S,m} \boldsymbol{\Omega}_{(1,A)} \mathbf{w}_B\right|^2$$

$$+ \sum_{l=1}^{L} \left|\mathbf{v}_{S,m}^H \mathbf{Z}_{S,lm} \mathbf{w}_{J,l}\right|^2 + \left|\mathbf{v}_{S,m}^H \mathbf{n}_{S,m}\right|^2,$$

And the wiretapped achievable rate of the r-th Eve on the CUs and the m-th ES are, respectively, written as[4]

$$R_{B,r} = \log_2\left(1 + \frac{\left|\mathbf{h}_{E,r}^H \boldsymbol{\Omega}_{(1,A)} \mathbf{w}_B\right|^2}{\sum_{m=1}^{M} \left|\mathbf{f}_{E,r}^H \mathbf{w}_{H,m}\right|^2 + \sigma_{E,r}^2}\right), \quad (7)$$

$$R_{H,rm} = \log_2\left(1 + \frac{\left|\mathbf{f}_{E,r}^H \mathbf{w}_{H,m}\right|^2}{\sum_{i\neq m}^{M} \left|\mathbf{f}_{E,r}^H \mathbf{w}_{H,i}\right|^2 + \left|\mathbf{h}_{E,r}^H \boldsymbol{\Omega}_{(1,A)} \mathbf{w}_B\right|^2 + \sigma_{E,r}^2}\right). \quad (8)$$

Moreover, the total power consumption P_{tot} of the considered secure ITAN can be formulated as

$$P_{tot} = \eta_1 \sum_{m=1}^{M} \|\mathbf{w}_{H,m}\|^2 + \eta_2 \|\mathbf{w}_B\|^2 + P_B + P_H, \quad (9)$$

$$P_B = (N_{RF} + KN_C) P_{rc} + (AN_R) P_{ris} + P_{bb}, \quad (10)$$

$$P_H = (N_H + MN_S) P_{rc} + P_{hb}, \quad (11)$$

where $\eta_1 > 1$ and $\eta_2 > 1$ are the power amplifier inefficiency of the BS and HAP, P_{rc} and P_{ris} denote the power consumption of the RF chains and RIS units, and P_{bb} and P_{hb} are the power consumed by baseband processor of the BS and HAP.

D. Channel Model

In the secure ITAN, there are two types of channels: the near-field channel and the far-field channel. The feeds-RIS and RIS-RIS channel are termed as the near-field channel, which can be characterized as the geometric radar model [14]. Thus, the near-field channel bwtween a-th layer and $(a-1)$-th layer

---

[4]According to [21], since the jammers and the eavesdroppers are cooperative communication parties, the jammers can utilize the multi-antenna technique to position the eavesdroppers in the null space of the jamming signal, and the eavesdroppers can also use the signal processing methods to eliminate the interference. Thus, it is reasonable to consider the worst case that the eavesdroppers can nullify the jamming signals, which leads to the wiretapped rate achieves the maximum.

(or the feeds when $a = 1$) can be expressed as [14]

$$\mathbf{B}_a = \left[\frac{\lambda \sqrt{\rho G_{u,v}^D \left(\theta^R, \varphi^R\right) G_{u,v}^R \left(\theta^D, \varphi^D\right)}}{4\pi d_{u,v}} e^{-j\frac{2\pi d_{u,v}}{\lambda}} \right]_{u,v}, \quad (12)$$

where λ is the wavelength, ρ denotes the power efficiency of RIS, $d_{u,v}$ is the distance between the (u,a)-th unit and the $(v, a-1)$-th unit, and $G_{u,v}^D \left(\theta^R, \varphi^R\right)$, $G_{u,v}^R \left(\theta^D, \varphi^D\right)$ are the active and passive antenna gains from the (u,a)-th unit and the $(v, a-1)$-th unit, respectively. Here, the symbol (i,j)-th unit denotes the i-th RIS units on the j-th layer. Besides, $\mathbf{B}_a$ depends on the illumination strategies, including relative orientation and positioning of (u,a)-th unit and the $(v, a-1)$-th unit. According to [14], the uniform separate illumination (USI) has superior performance than other illumination strategies, thus we directly adopt USI to illuminate each RIS layer. As such, $\mathbf{B}_a$ can be simplified to

$$\mathbf{B}_a = \left[\chi_a e^{-j\frac{2\pi d_{u,v}}{\lambda}} \right]_{u,v}, \quad (13)$$

with

$$\chi_a = \begin{cases} \frac{\lambda}{4\pi d} \sqrt{\frac{4\pi\rho}{1-\cos\left(\theta_0^{SI}\right)}}, & n \in N_R \\ 0 & \text{otherwise} \end{cases},$$

where d is the average distance between the units on a-th layer and the units on $(a+1)$-th layer, and θ_0^{SI} denotes the illumination angle. Note that $\mathbf{B}_a$ is a fixed matrix and can be precisely measured, due to the fact that the distance between adjacent vertical layers is very short [25]. In addition, the RIS's power loss is implicitly captured by $\mathbf{B}_a$, i.e., the power efficiency ρ, which includes spillover loss, taper loss, and aperture loss [14].

As for the terrestrial and aerial downlink channels, it can be regarded as the far-field channel, which can be modeled as the superposition of a predominant line-of-sight (LoS) component and a sparse set of single-bounce non-LoS (NLoS) components [26]. Thus, the downlink channels are written as

$$\mathbf{Z} = \mathbf{H} = \mathbf{F} = g_0 \mathbf{a}_P \left(\theta_0^R, \varphi_0^R\right) \mathbf{a}_P^H \left(\theta_0^T, \varphi_0^T\right)$$
$$+ \sqrt{\frac{1}{PL}} \sum_{d=1}^{PL} g_d \mathbf{a}_P \left(\theta_d^R, \varphi_d^R\right) \mathbf{a}_P^H \left(\theta_d^T, \varphi_d^T\right), \quad (14)$$

$$\mathbf{h} = \mathbf{f} = g_0 \mathbf{a}_P \left(\theta_0^T, \varphi_0^T\right) + \sqrt{\frac{1}{PL}} \sum_{d=1}^{PL} g_d \mathbf{a}_P \left(\theta_d^T, \varphi_d^T\right), \quad (15)$$

where PL is the total number of multiple paths, θ^T (θ^R) is the vertical AoD (AoA), and φ^T (φ^R) denote the horizontal AoD (AoA). g represents the large-scale fading coefficients, and $g \sim \mathcal{CN}(0, 10^{Loss/10})$, where $Loss = -30.18 - 26 \log 10 \left(d_s\right)$[dB] and d_s is the link distance. In addition, $\mathbf{a}_P \left(\theta, \varphi\right)$ is the steering vectors of UPA, which is given by

$$\mathbf{a}_P \left(\theta, \varphi\right) = \left[1, e^{j\frac{2\pi d_1}{\lambda} \sin\theta \cos\varphi}, \cdots, e^{j\frac{2\pi d_1 (N_1-1)}{\lambda} \sin\theta \cos\varphi}\right]^T$$
$$\otimes \left[1, e^{j\frac{2\pi d_2}{\lambda} \cos\theta}, \cdots, e^{j\frac{2\pi d_2 (N_2-1)}{\lambda} \cos\theta}\right]^T, \quad (16)$$

where N_1/N_2 denotes the number of array elements along the UPA side, and d_1/d_2 is the inter-element spacing along the UPA side. In this paper, we set the inter-element spacing as the half-wavelength, i.e., $d_1 = d_2 = \lambda/2$.

Since the CUs/ESs can send pilot signals to BS/HAP for facilitating the channel estimation, the system has ability to periodically obtian the CSI of the legitimate nodes [20]. In the

recent works, there are several channel estimation techniques to acquire the accurate CSI in the RIS-assisted systems, e.g., [27]. Therefore, we assume that all the involved legitimate CSI, i.e., $\mathbf{H}_{C,k}$, $\mathbf{H}_{S,m}$, $\mathbf{F}_{C,k}$, and $\mathbf{F}_{S,m}$, can be accurately obtained during the whole transmission period. However, as the malicious jammer and the potential eavesdroppers are not expected to cooperate with the system for the CSI estimation, we further assume that the accurate illegitimate CSI, i.e., $\mathbf{Z}_{C,lk}$, $\mathbf{Z}_{S,lm}$, $\mathbf{h}_{E,r}$, and $\mathbf{f}_{E,r}$, is unavailable to the system. To account for this effect, we suppose that the illegitimate CSI belong to a given AoA-based range, which is given by[5]

$$\Delta_{J,l} = \Big\{ \mathbf{Z}_{C,lk}, \mathbf{Z}_{S,lm} \big| \theta_{lk}^Z \in \big[\theta_{lk,L}^Z, \theta_{lk,U}^Z\big], \theta_{lm}^Z \in \big[\theta_{lm,L}^Z, \theta_{lm,U}^Z\big]$$
$$\varphi_{lk}^Z \in \big[\varphi_{lk,L}^Z, \varphi_{lk,U}^Z\big], \varphi_{lm}^Z \in \big[\varphi_{lm,L}^Z, \varphi_{lm,U}^Z\big], |g_{lk}^Z| \in$$
$$\big[g_{lk,L}^Z, g_{lk,U}^Z\big], |g_{lm}^Z| \in \big[g_{lm,L}^Z, g_{lm,U}^Z\big] \Big\}, \forall l, k, m, \quad (17)$$

$$\Delta_{E,r} = \Big\{ \mathbf{h}_{E,r}, \mathbf{f}_{E,r} \big| \theta_r^h \in \big[\theta_{r,L}^h, \theta_{r,U}^h\big], \theta_r^f \in \big[\theta_{r,L}^f, \theta_{r,U}^f\big], \varphi_r^h \in \big[\varphi_{r,L}^h, \varphi_{r,U}^h\big]$$
$$\varphi_r^f \in \big[\varphi_{r,L}^f, \varphi_{r,U}^f\big], |g_r^h| \in \big[g_{r,L}^h, g_{r,U}^h\big], |g_r^f| \in \big[g_{r,L}^f, g_{r,U}^f\big] \Big\}, \forall r, \quad (18)$$

where θ_U and θ_L denote the upper and lower bounds of vertical AoD (AoA), φ_U and φ_L are the upper and lower bounds of horizontal AoD (AoA), and g_U and g_L is the upper and lower bounds of the channel gain amplitude.

E. Problem Formulation

In this paper, a worst-case energy efficiency (EE) maximization problem is formulated, where the EE is defined as the ratio of the sum weighted achievable rate to the power consumption. Specifically, under the CSI uncertainties Δ_J, Δ_E and both jamming and eavesdropping attacks, we aim to maximize the worst-case EE by jointly designing the received precoder $\mathbf{v}_{C,k}$, $\mathbf{v}_{S,m}$, digital precoder $\mathbf{w}_B$, $\mathbf{w}_{H,m}$, and analog precoder $\mathbf{P}_a$, while meeting the rate requirements, transmit power constraints and RIS unit-modula constraint. Thus, the corresponding problem can be formulated as

$$\max_{\substack{\mathbf{w}_B, \mathbf{P}_a, \mathbf{w}_{H,m}, \Delta_J \\ \mathbf{v}_{C,k}, \mathbf{v}_{S,m}}} \min \left(\sum_{k=1}^K \mu_{C,k} R_{C,k} + \sum_{m=1}^M \mu_{S,m} R_{S,m} \right) \Big/ P_{tot} \quad (19a)$$

$$s.t. \quad \min_{\Delta_J} R_{C,k} \geq \Gamma_{C,k}, \forall k, \quad (19b)$$

$$\min_{\Delta_J} R_{S,m} \geq \Gamma_{S,m}, \forall m, \quad (19c)$$

$$\max_{\Delta_E} R_{B,r} \leq \Gamma_{B,r}, \forall r, \quad (19d)$$

$$\max_{\Delta_E} R_{E,rm} \leq \Gamma_{E,rm}, \forall r, m, \quad (19e)$$

$$\|\mathbf{w}_B\|^2 \leq P_{B,\max}, \quad \sum_{m=1}^M \|\mathbf{w}_{H,m}\|^2 \leq P_{H,\max}, \quad (19f)$$

$$\big|[\mathbf{P}_a]_{i,i}\big| = 1, a = 1, \cdots, A, i = 1, \cdots, N_R, \quad (19g)$$

$$\|\mathbf{v}_{C,k}\|^2 = 1, \forall k, \quad (19h)$$

$$\|\mathbf{v}_{S,m}\|^2 = 1, \forall m, \quad (19i)$$

where $\mu_{C,k}$ and $\mu_{S,m}$ are the positive weighted factor of k-th CU and m-th ES, $\Gamma_{C,k}$, $\Gamma_{S,m}$, $\Gamma_{B,r}$, and $\Gamma_{E,rm}$ are the

---

[5]Note that the imperfect angular information based CSI model in (14) and (15) can characterize the channel more accurately than the widely adopted statistical or bounded uncertainty model, which is only suitable for the uncorrelated Rayleigh fading channels without LoS signal component [8].

rate target for k-th CU, m-th ES, and l-th Eve, and $P_{B,\max}$, $P_{H,\max}$ are the maximum power in the BS and HAP side.

Different from the existing digital beamforming scheme which has been widely adopted to solve EE maximization problems [28], the multi-layer RIS-assisted hybrid beamforming scheme is a more general form involving both analog and digital beamforming optimization problem. Besides, the existing schemes for optimizing the digital beamforming cannot be directly extended to solve the abovementioned complex problem due to the non-convex objective function with coupled variables, and the non-convex constraints on the RIS elements of the analog precoder. Moreover, the imperfect angular information based CSI leads to infinite non-convex constraints in both the objective function and the constraints, which constitutes another challenge for solving (19).

III. MULTI-LAYER RIS-ASSISTED HYBRID SECURE BEAMFORMING DESIGN

In this section, we adopt the block coordinate descent (BCD) method to solve the intractable problem (19) and thus obtain the received precoder, digital precoder, and RIS-aided analog precoder in an iterative manner.

A. Heuristic Beamforming Scheme for $\mathbf{v}_{C,k}$ and $\mathbf{v}_{S,m}$

First, the optimization of the received precoder $\mathbf{v}_{C,k}$ and $\mathbf{v}_{S,m}$ are investigated. Note that $\mathbf{v}_{C,k}$ and $\mathbf{v}_{S,m}$ only determine the achievable rate $R_{C,k}$ and $R_{S,m}$, respectively, and thus we should only optimize $\mathbf{v}_{C,k}$ and $\mathbf{v}_{S,m}$ to maximize $R_{C,k}$ and $R_{S,m}$ in this subsection. In this regard, by dropping the monotonic increasing function $\log_2(.)$ in $R_{C,k}$ and $R_{S,m}$, the corresponding optimization problem can be expressed as the following worst-case problems

$$\max_{\mathbf{v}_{C,k}} \min_{\mathbf{Z}_{C,lk} \in \Delta_J} \left| \mathbf{v}_{C,k}^H \mathbf{H}_{C,k} \mathbf{\Omega}_{(1,A)} \mathbf{w}_B \right|^2 \Big/ \beta_{C,k} \ s.t.(19h). \quad (20)$$

$$\max_{\mathbf{v}_{S,m}} \min_{\mathbf{Z}_{S,lm} \in \Delta_J} \left| \mathbf{v}_{S,m}^H \mathbf{F}_{S,m} \mathbf{w}_{H,m} \right|^2 \Big/ \beta_{S,m} \quad s.t.\ (19i). \quad (21)$$

However, since the system can obtain neither the instantaneous CSI $\mathbf{Z}_{C,lk}$, $\mathbf{Z}_{S,lm}$ nor the jamming beamforming $\mathbf{w}_{J,l}$ insides $\beta_{C,k}$ and $\beta_{S,m}$, the problem (20) and (21) are still challenging to solve. To ensure the problems is feasible, we first utilize the Cauchy-Schwarz inequality to obtain the upper bound of received jamming power insides $\beta_{C,k}$ and $\beta_{S,m}$, i.e.,

$$\sum_{l=1}^{L} \left| \mathbf{v}_{C,k}^H \mathbf{Z}_{C,lk} \mathbf{w}_{J,l} \right|^2 \leq \sum_{l=1}^{L} \widehat{p}_{J,l} \left\| \mathbf{v}_{C,k}^H \mathbf{Z}_{C,lk} \right\|^2, \quad (22)$$

$$\sum_{l=1}^{L} \left| \mathbf{v}_{S,m}^H \mathbf{Z}_{S,lm} \mathbf{w}_{J,l} \right|^2 \leq \sum_{l=1}^{L} \widehat{p}_{J,l} \left\| \mathbf{v}_{S,m}^H \mathbf{Z}_{S,lm} \right\|^2, \quad (23)$$

where $\widehat{p}_{J,l}$ denotes the the estimation of the BSs transmit power, which can be obtained by the rotational invariance techniques [29]. As such, the unknown $\mathbf{w}_{J,l}$ is addressed and after some mathematical transformations, we can tranform (20) and (21) into

$$\max_{\mathbf{v}_{C,k}} \min_{\Lambda_{C,k}} \frac{\mathbf{v}_{C,k}^H \mathbf{A}_{C,k} \mathbf{v}_{C,k}}{\mathbf{v}_{C,k}^H \mathbf{D}_{C,k} \mathbf{v}_{C,k}} \quad s.t.\ (19h), \quad (24)$$

$$\max_{\mathbf{v}_{S,m}} \min_{\Lambda_{S,m}} \frac{\mathbf{v}_{S,m}^H \mathbf{\Xi}_{S,mm} \mathbf{v}_{S,m}}{\mathbf{v}_{S,m}^H \mathbf{D}_{S,m} \mathbf{v}_{S,m}} \quad s.t.\ (19i), \quad (25)$$

where

$$\mathbf{D}_{C,k} = \sum_{m=1}^{M} \mathbf{\Xi}_{C,km} + \sum_{l=1}^{L} \widehat{p}_{J,l} \mathbf{\Psi}_{C,lk} + \sigma_{C,k}^2 \mathbf{I},$$

$$\mathbf{D}_{S,m} = \mathbf{A}_{S,m} + \sum_{i \neq m}^{M} \mathbf{\Xi}_{S,mi} + \sum_{l=1}^{L} \widehat{p}_{J,l} \mathbf{\Psi}_{S,lm} + \sigma_{S,m}^2 \mathbf{I},$$

$$\mathbf{A}_{C,k} = \mathbf{a}_{C,k} \mathbf{a}_{C,k}^H = \mathbf{H}_{C,k} \mathbf{\Omega}_{(1,A)} \mathbf{w}_B \left(\mathbf{H}_{C,k} \mathbf{\Omega}_{(1,A)} \mathbf{w}_B \right)^H,$$

$$\mathbf{A}_{S,m} = \mathbf{H}_{S,m} \mathbf{\Omega}_{(1,A)} \mathbf{w}_B \left(\mathbf{H}_{S,m} \mathbf{\Omega}_{(1,A)} \mathbf{w}_B \right)^H,$$

$$\mathbf{\Xi}_{C,km} = \mathbf{F}_{C,k} \mathbf{w}_{H,m} (\mathbf{F}_{C,k} \mathbf{w}_{H,m})^H,$$

$$\mathbf{\Xi}_{S,mi} = \boldsymbol{\xi}_{S,mi} \boldsymbol{\xi}_{S,mi}^H = \mathbf{F}_{S,m} \mathbf{w}_{H,i} (\mathbf{F}_{S,m} \mathbf{w}_{H,i})^H,$$

$$\mathbf{\Psi}_{C,lk} = \mathbf{Z}_{C,lk} \mathbf{Z}_{C,lk}^H, \ \mathbf{\Psi}_{S,lm} = \mathbf{Z}_{S,lm} \mathbf{Z}_{S,lm}^H,$$

$$\Lambda_{C,k} = \left\{ \mathbf{\Psi}_{C,lk} \big| \theta_{lk}^Z \in \left[\theta_{lk,L}^Z, \theta_{lk,U}^Z \right], \varphi_{lk}^Z \in \left[\varphi_{lk,L}^Z, \varphi_{lk,U}^Z \right], \right.$$
$$\left. \left| g_{lk}^Z \right| \in \left[g_{lk,L}^Z, g_{lk,U}^Z \right], \forall l \right\}, \Lambda_{S,m} = \left\{ \mathbf{\Psi}_{S,lm} \big| \theta_{lm}^Z \in \left[\theta_{lm,L}^Z, \theta_{lm,U}^Z \right], \right.$$
$$\left. \varphi_{lm}^Z \in \left[\varphi_{lm,L}^Z, \varphi_{lm,U}^Z \right], \left| g_{lm}^Z \right| \in \left[g_{lm,L}^Z, g_{lm,U}^Z \right], \forall l \right\}.$$

However, the problems (24) and (25) are still difficult to solve due to the imperfect jammer's CSI induced by $\Lambda_{C,k}$ and $\Lambda_{S,m}$. To address the issue such that the worst case is achieved, we formulate the convex hull of $\Lambda_{C,k}$ and $\Lambda_{S,m}$, respectively, as

$$\Psi_{C,k} = \left\{ \sum_{i=1}^{Q_{C,k}} \alpha_{C,lki} \mathbf{\Psi}_{C,lki} \Bigg| \sum_{i=1}^{Q_{C,k}} \alpha_{C,lki} = 1, \alpha_{C,lki} \geq 0, \forall l \right\}, \forall k, \ (26)$$

$$\Psi_{S,m} = \left\{ \sum_{i=1}^{Q_{S,m}} \alpha_{S,lmi} \mathbf{\Psi}_{S,lmi} \Bigg| \sum_{i=1}^{Q_{S,m}} \alpha_{S,lmi} = 1, \alpha_{S,lmi} \geq 0, \forall l \right\}, \forall m, (27)$$

where $\alpha_{C,lki}$, $\alpha_{S,lmi}$ is the weighted coefficient, $\mathbf{\Psi}_{C,lki}$, $\mathbf{\Psi}_{S,lmi}$ denotes the i-th discrete element in the convex hull $\Lambda_{C,k}$, $\Lambda_{S,m}$, and $Q_{C,k}$, $Q_{S,m}$ represents the number of samples of $\Lambda_{C,k}$, $\Lambda_{S,m}$. To proceed on, the following two propositions are needed.

Proposition 1: The objective functions insides (24) and (25) with $\Lambda_{C,k}$ and $\Lambda_{S,m}$ can be equivalently transformed into that with $\Psi_{C,k}$ and $\Psi_{S,m}$, i.e.,

$$\max_{\mathbf{v}_{C,k}} \min_{\Lambda_{C,k}} \frac{\mathbf{v}_{C,k}^H \mathbf{A}_{C,k} \mathbf{v}_{C,k}}{\mathbf{v}_{C,k}^H \mathbf{D}_{C,k} \mathbf{v}_{C,k}} = \max_{\mathbf{v}_{C,k}} \min_{\Psi_{C,k}} \frac{\mathbf{v}_{C,k}^H \mathbf{A}_{C,k} \mathbf{v}_{C,k}}{\mathbf{v}_{C,k}^H \mathbf{D}_{C,k} \mathbf{v}_{C,k}}, \quad (28)$$

$$\max_{\mathbf{v}_{S,m}} \min_{\Lambda_{S,m}} \frac{\mathbf{v}_{S,m}^H \mathbf{\Xi}_{S,mm} \mathbf{v}_{S,m}}{\mathbf{v}_{S,m}^H \mathbf{D}_{S,m} \mathbf{v}_{S,m}} = \max_{\mathbf{v}_{S,m}} \min_{\Psi_{S,m}} \frac{\mathbf{v}_{S,m}^H \mathbf{\Xi}_{S,mm} \mathbf{v}_{S,m}}{\mathbf{v}_{S,m}^H \mathbf{D}_{S,m} \mathbf{v}_{S,m}}. \quad (29)$$

Proof: Please refer to Appendix A. ∎

Proposition 2: The max-min problems (28) and (29) is equivalent to the following min-max problem, namely,

$$\max_{\mathbf{v}_{C,k}} \min_{\Psi_{C,k}} \frac{\mathbf{v}_{C,k}^H \mathbf{A}_{C,k} \mathbf{v}_{C,k}}{\mathbf{v}_{C,k}^H \mathbf{D}_{C,k} \mathbf{v}_{C,k}} = \min_{\Psi_{C,k}} \max_{\mathbf{v}_{C,k}} \frac{\mathbf{v}_{C,k}^H \mathbf{A}_{C,k} \mathbf{v}_{C,k}}{\mathbf{v}_{C,k}^H \mathbf{D}_{C,k} \mathbf{v}_{C,k}}, \quad (30)$$

$$\max_{\mathbf{v}_{S,m}} \min_{\Psi_{S,m}} \frac{\mathbf{v}_{S,m}^H \mathbf{\Xi}_{S,mm} \mathbf{v}_{S,m}}{\mathbf{v}_{S,m}^H \mathbf{D}_{S,m} \mathbf{v}_{S,m}} = \min_{\Psi_{S,m}} \max_{\mathbf{v}_{S,m}} \frac{\mathbf{v}_{S,m}^H \mathbf{\Xi}_{S,mm} \mathbf{v}_{S,m}}{\mathbf{v}_{S,m}^H \mathbf{D}_{S,m} \mathbf{v}_{S,m}}. \quad (31)$$

Proof: Please refer to Appendix B. ∎

According to *Proposition 1*, *Proposition 2* and using the convex hull in (26), (27), the intractable problems (24) and (25) can be equivalently reformulated as

$$\min_{\{\alpha_{C,lki}\}} \max_{\mathbf{v}_{C,k}} \frac{\mathbf{v}_{C,k}^H \mathbf{A}_{C,k} \mathbf{v}_{C,k}}{\mathbf{v}_{C,k}^H \overline{\mathbf{D}}_{C,k} \mathbf{v}_{C,k}} \quad s.t.\ (19h), \quad (32)$$

$$\min_{\{\alpha_{S,lmi}\}} \max_{\mathbf{v}_{S,m}} \frac{\mathbf{v}_{S,m}^H \mathbf{\Xi}_{S,mm} \mathbf{v}_{S,m}}{\mathbf{v}_{S,m}^H \overline{\mathbf{D}}_{S,m} \mathbf{v}_{S,m}} \quad s.t. \ (19i), \qquad (33)$$

where

$$\overline{\mathbf{D}}_{C,k} = \sum_{m=1}^{M} \mathbf{\Xi}_{C,km} + \sum_{l=1}^{L} \widehat{p}_{J,l} \sum_{i=1}^{Q_{C,k}} \alpha_{C,lki} \mathbf{\Psi}_{C,lki} + \sigma_{C,k}^2 \mathbf{I},$$

$$\overline{\mathbf{D}}_{S,m} = \mathbf{A}_{S,m} + \sum_{i \neq m}^{M} \mathbf{\Xi}_{S,mi} + \sum_{l=1}^{L} \widehat{p}_{J,l} \sum_{i=1}^{Q_{S,m}} \alpha_{S,lmi} \mathbf{\Psi}_{S,lmi} + \sigma_{S,m}^2 \mathbf{I}.$$

Then, to obtain the analytical beamfoming weight vectors, given $\{\alpha_{C,lki}\}$ and $\{\alpha_{S,lmi}\}$, the optimization problems with generalized Rayleigh quotient form can be obtained as

$$\max_{\mathbf{v}_{C,k}} \frac{\mathbf{v}_{C,k}^H \mathbf{A}_{C,k} \mathbf{v}_{C,k}}{\mathbf{v}_{C,k}^H \overline{\mathbf{D}}_{C,k} \mathbf{v}_{C,k}} \quad s.t. \ (19h), \qquad (34)$$

$$\max_{\mathbf{v}_{S,m}} \frac{\mathbf{v}_{S,m}^H \mathbf{\Xi}_{S,mm} \mathbf{v}_{S,m}}{\mathbf{v}_{S,m}^H \overline{\mathbf{D}}_{S,m} \mathbf{v}_{S,m}} \quad s.t. \ (19i). \qquad (35)$$

Clearly, the optimal solution to (34) and (35) is given by

$$\mathbf{v}_{C,k} = \mathrm{eig}\left(\mathbf{A}_{C,k}, \overline{\mathbf{D}}_{C,k}\right), \gamma_{C,k} = \lambda_{\max}\left(\mathbf{A}_{C,k}, \overline{\mathbf{D}}_{C,k}\right), \quad (36)$$

$$\mathbf{v}_{S,m} = \mathrm{eig}\left(\mathbf{A}_{S,m}, \overline{\mathbf{D}}_{S,m}\right), \gamma_{S,m} = \lambda_{\max}\left(\mathbf{A}_{S,m}, \overline{\mathbf{D}}_{S,m}\right), \quad (37)$$

where $\lambda_{\max}\left(\mathbf{A}, \mathbf{D}\right)$ is the largest generalized eigenvalue of the matrix pair $(\mathbf{A}, \mathbf{D})$, and $\mathrm{eig}\left(\mathbf{A}, \mathbf{D}\right)$ denotes the corresponding principle generalized eigenvector.

Proposition 3: The optimal solution (36) and (37) can be further simplified, respectively, as

$$\mathbf{v}_{C,k} = \frac{\overline{\mathbf{D}}_{C,k}^{\dagger} \mathbf{a}_{C,k}}{\left\| \overline{\mathbf{D}}_{C,k}^{\dagger} \mathbf{a}_{C,k} \right\|}, \gamma_{C,k} = \mathbf{a}_{C,k}^H \overline{\mathbf{D}}_{C,k}^{\dagger} \mathbf{a}_{C,k}, \qquad (38)$$

$$\mathbf{v}_{S,m} = \frac{\overline{\mathbf{D}}_{S,m}^{\dagger} \boldsymbol{\xi}_{S,mm}}{\left\| \overline{\mathbf{D}}_{S,m}^{\dagger} \boldsymbol{\xi}_{S,mm} \right\|}, \gamma_{S,m} = \boldsymbol{\xi}_{S,mm}^H \overline{\mathbf{D}}_{S,m}^{\dagger} \boldsymbol{\xi}_{S,mm}. \qquad (39)$$

Proof: Please refer to Appendix C. ∎

By using the ***Proposition 3***, an alternative expression of (36) and (37) can be utilized to reduce the computational complex of the algorithm. Then, we aim to choose $\{\alpha_{C,lki}\}$ and $\{\alpha_{S,lmi}\}$ for minimizing the objective function (32) and (33), respectively, such that the worst case is achieved. By utilizing the Cauchy-Schwarz inequality, we can obtain that

$$\left(\sum_{i=1}^{Q_{C,k}} \alpha_{C,lki} \mathbf{v}_{C,k}^H \mathbf{\Psi}_{C,lki} \mathbf{v}_{C,k} \right)^2$$

$$\leq \left(\sum_{i=1}^{Q_{C,k}} \alpha_{C,lki}^2 \right) \left(\sum_{i=1}^{Q_{C,k}} \left(\mathbf{v}_{C,k}^H \mathbf{\Psi}_{C,lki} \mathbf{v}_{C,k} \right)^2 \right), \qquad (40)$$

$$\left(\sum_{i=1}^{Q_{S,m}} \alpha_{S,lmi} \mathbf{v}_{S,m}^H \mathbf{\Psi}_{S,lmi} \mathbf{v}_{S,m} \right)^2$$

$$\leq \left(\sum_{i=1}^{Q_{S,m}} \alpha_{S,lmi}^2 \right) \left(\sum_{i=1}^{Q_{S,m}} \left(\mathbf{v}_{S,m}^H \mathbf{\Psi}_{S,lmi} \mathbf{v}_{S,m} \right)^2 \right). \qquad (41)$$

Obviously, the equality hold only when $\frac{\alpha_{C,lk1}}{\mathbf{v}_{C,k}^H \mathbf{\Psi}_{C,lk1} \mathbf{v}_{C,k}} = \frac{\alpha_{C,lk2}}{\mathbf{v}_{C,k}^H \mathbf{\Psi}_{C,lk2} \mathbf{v}_{C,k}} = \cdots = \frac{\alpha_{C,lkQ_{C,k}}}{\mathbf{v}_{C,k}^H \mathbf{\Psi}_{C,lkQ_{C,k}} \mathbf{v}_{C,k}}$ and $\frac{\alpha_{S,lm1}}{\mathbf{v}_{S,m}^H \mathbf{\Psi}_{S,lm1} \mathbf{v}_{S,m}} = \frac{\alpha_{S,lm2}}{\mathbf{v}_{S,m}^H \mathbf{\Psi}_{S,lm2} \mathbf{v}_{S,m}} = \cdots = \frac{\alpha_{S,lmQ_{S,m}}}{\mathbf{v}_{S,m}^H \mathbf{\Psi}_{S,lmQ_{S,m}} \mathbf{v}_{S,m}}$. In order to achieve the worst-case achievable rate in (20) and

(21), $\{\alpha_{C,lki}\}$ and $\{\alpha_{S,lmi}\}$ should be chosen as

$$\alpha_{C,lki} = \frac{\mathbf{v}_{C,k}^H \mathbf{\Psi}_{C,lki} \mathbf{v}_{C,k}}{\sum\limits_{i=1}^{Q_{C,k}} \mathbf{v}_{C,k}^H \mathbf{\Psi}_{C,lki} \mathbf{v}_{C,k}}, \forall i, \qquad (42)$$

$$\alpha_{S,lmi} = \frac{\mathbf{v}_{S,m}^H \mathbf{\Psi}_{S,lmi} \mathbf{v}_{S,m}}{\sum\limits_{i=1}^{Q_{C,k}} \mathbf{v}_{S,m}^H \mathbf{\Psi}_{S,lmi} \mathbf{v}_{S,m}}, \forall i. \qquad (43)$$

Finally, the optimal $\mathbf{v}_{C,k}$ and $\mathbf{v}_{S,m}$ can be obtained in an iterative manner using the method proposed in Section III-A.

B. Sequential Convex Approximation for $\mathbf{w}_B$ and $\mathbf{w}_{H,m}$

In this subsection, we aim to solve $\mathbf{w}_B$ and $\mathbf{w}_{H,m}$ with given $\mathbf{v}_{C,k}$, $\mathbf{v}_{S,m}$ and $\mathbf{P}_a$. However, the initial optimazation problem (19) is challenging to solve due to the non-convex objective function and infinite non-convex uncertainties Δ_J and Δ_E, thus we first develop a novel discretization method to tackle the continuous uncertainties, and then a method based on sequential convex approximation (SCA) is proposed to solve the intractable problem.

First, we focus on addressing the CSI uncertainties. In terms of Δ_J, since the jamming power $\sum_{l=1}^{L} \left| \mathbf{v}_{C,k}^H \mathbf{Z}_{C,lk} \mathbf{w}_{J,l} \right|^2$ and $\sum_{l=1}^{L} \left| \mathbf{v}_{S,m}^H \mathbf{Z}_{S,lm} \mathbf{w}_{J,l} \right|^2$ in (5) and (6) involves no terms of $\mathbf{w}_B$, $\mathbf{w}_{H,m}$, we can regard it as a fixed power in the subsection, and thus the term $\min_{\Delta_J}$ insides (19a)-(19c) can be directly removed. As for Δ_E, we first let $\left| g_r^h \right| = \left| g_{r,U}^h \right|$ and $\left| g_r^f \right| = \left| g_{r,U}^f \right|, \forall k, m, l, r$ so that the wiretap rate is maximal. Then, we utilize the following discretization method to form the worst-case Eve's CSI. Specifically, any continuous uncertainty Δ_g can be expressed as

$$\Delta_g = \{\mathbf{G}_1, \cdots, \mathbf{G}_{Sa}\}, \qquad (44)$$

where $\mathbf{G}_n$ is one possible channel in Δ_g and Sa denotes the discrete sample number. Note that the discrete-form uncertainty is a general form due to the fact that Sa can be taken as infinity. Here, we can use the following sample method to discrete Δ_g. According to [30], since only angular information based uncertainty region is known, the angle in the set of Δ_g can be uniformly selected, which is given by

$$\theta^{(i)} = \theta_L + (i-1)\Delta\theta, \ i = 1, \cdots, Q_1, \qquad (45)$$

$$\varphi^{(j)} = \varphi_L + (j-1)\Delta\varphi, \ j = 1, \cdots, Q_2, \qquad (46)$$

where $\left\{\theta^{(i)}, \varphi^{(j)}\right\}$ are the angular information of $\mathbf{G}^{(i,j)}$, $Q_1 \geq N_1$ and $Q_2 \geq N_2$ denote the sample number of θ and φ, and $\Delta\theta = (\theta_U - \theta_L)/(Q_1-1)$, $\Delta\varphi = (\varphi_U - \varphi_L)/(Q_2-1)$. Then, the discrete uncertainty of channel matrix can be expressed as

$$\widehat{\Delta}_g = \left\{\mathbf{G}_1 \mathbf{G}_1^H, \cdots, \mathbf{G}_{Sa} \mathbf{G}_{Sa}^H\right\}. \qquad (47)$$

Thus, any imperfect CSI in angular uncertainty set Δ_g can be expressed as the combination of discrete elements in (47), which is consistent with (26) and (27). As such, we can obtain the worst-case Eve's CSI, namely,

$$\widetilde{\mathbf{F}}_{E,r} = \sum_{i=1}^{N_{S1}} \sum_{j=1}^{N_{S2}} \alpha_{F,ij} \mathbf{f}_{E,r}^{(i,j)} \mathbf{f}_{E,r}^{(i,j),H}, \qquad (48)$$

$$\widetilde{\mathbf{G}}_{E,r} = \sum_{i=1}^{N_{R1}} \sum_{j=1}^{N_{R1}} \alpha_{G,ij} \mathbf{g}_{E,r}^{(i,j)} \mathbf{g}_{E,r}^{(i,j),H}, \qquad (49)$$

where $N_R = N_{R1} \times N_{R2}$, $N_S = N_{S1} \times N_{S2}$, and $\mathbf{g}_{E,r} = \mathbf{\Omega}_{(1,A)}^H \mathbf{h}_{E,r}$. To make the EE at its maximum for all possible

channel errors, according to [8], [9], [30], [31], $\alpha_{G,ij}=1/N_R$ and $\alpha_{F,ij}=1/N_S$ should be choosen to achieve the worst case. As such, the $\max_{\Delta_E}$ in (19d) and (19e) can be removed.

Then, we turn to tackle the non-convex objective function (19a). By introducing a positive auxiliary variable t into objective function and after some mathematical transformations, the optimzation problem on $\mathbf{w}_B$, $\mathbf{w}_{H,m}$ can be rewritten as

$$\max_{\mathbf{w}_B,\mathbf{w}_{H,m},t} t \tag{50a}$$

$$s.t. \ (19b)^*, (19c)^*, (19f), \tag{50b}$$

$$\left(\sum_{k=1}^{K}\mu_{C,k}R_{C,k}+\sum_{m=1}^{M}\mu_{S,m}R_{S,m}\right)\Big/P_{tot}\geq\sqrt{t}, \tag{50c}$$

$$\widetilde{\Gamma}_{B,r}\mathrm{Tr}\left\{\widetilde{\mathbf{G}}_{E,r}\mathbf{W}_B\right\}-\sum_{m=1}^{M}\mathrm{Tr}\left\{\widetilde{\mathbf{F}}_{E,r}\mathbf{W}_{H,m}\right\}\leq\sigma_{E,r}^2,\forall r, \tag{50d}$$

$$\widetilde{\Gamma}_{E,rm}\mathrm{Tr}\left\{\widetilde{\mathbf{F}}_{E,r}\mathbf{W}_{H,m}\right\}-\sum_{i\neq m}^{M}\mathrm{Tr}\left\{\widetilde{\mathbf{F}}_{E,r}\mathbf{W}_{H,i}\right\}$$
$$-\mathrm{Tr}\left\{\widetilde{\mathbf{G}}_{E,r}\mathbf{W}_B\right\}-\sigma_{E,r}^2\leq 0,\forall r,m, \tag{50e}$$

where
$\widetilde{\Gamma}_{B,r}=1/\left(2^{\Gamma_{B,r}}-1\right),\widetilde{\Gamma}_{E,rm}=1/\left(2^{\Gamma_{E,rm}}-1\right)$,
$\mathbf{W}_B=\mathbf{w}_B^{(n-1)}\mathbf{w}_B^H+\mathbf{w}_B\mathbf{w}_B^{(n-1)H}-\mathbf{w}_B^{(n-1)}\mathbf{w}_B^{(n-1)H}$,
$\mathbf{W}_{H,m}=\mathbf{w}_{H,m}^{(n-1)}\mathbf{w}_{H,m}^H+\mathbf{w}_{H,m}\mathbf{w}_{H,m}^{(n-1)H}-\mathbf{w}_{H,m}^{(n-1)}\mathbf{w}_{H,m}^{(n-1)H}$.
and the constraint $(X)^*$ denotes the modified version of (X) without $\min_{\Delta_J}$. Here, $\mathbf{W}_B$ and $\mathbf{W}_{H,m}$ are obtained by the first-order Taylor series, and $s^{(n-1)}$ is the optimal solution obtained at the $(n-1)$-th iteration.

It is observed that there is an additional constraints (50c) introduced by the auxiliary variable t, which constitutes a challenge for solving the problem (50). To address the issue, by adding an auxiliary variable ς, the non-convex constraint (50c) with the auxiliary variable t can be equivalently be decomposed into

$$\sum_{k=1}^{K}\mu_{C,k}R_{C,k}+\sum_{m=1}^{M}\mu_{S,m}R_{S,m}\geq\sqrt{t\varsigma}, \tag{51}$$

$$\eta_1\sum_{m=1}^{M}\|\mathbf{w}_{H,m}\|^2+\eta_2\|\mathbf{w}_B\|^2+P_B+P_H\leq\sqrt{\varsigma}. \tag{52}$$

Nevertheless, the constraints (51) and (52) are sitll non-convex. To handle the non-convexity of (51), we first introduce a set of slack variables $\{\delta_{C,k}\}$, $\{\delta_{S,m}\}$ into it and obtain that

$$\sum_{k=1}^{K}\mu_{C,k}\delta_{C,k}+\sum_{m=1}^{M}\mu_{S,m}\delta_{S,m}\geq\sqrt{t\varsigma}, \tag{53}$$

$$R_{C,k}\geq\delta_{C,k},\forall k,\ R_{S,m}\geq\delta_{S,m},\forall m, \tag{54}$$

Then, replacing the concave term $\sqrt{t\varsigma}$ insides (53) with the first-order Taylor series, constraint (51) can be rewritten as

$$\sum_{k=1}^{K}\mu_{C,k}\delta_{C,k}+\sum_{m=1}^{M}\mu_{S,m}\delta_{S,m}\geq\sqrt{t^{(n-1)}\varsigma^{(n-1)}} \tag{55}$$
$$+\frac{1}{2}\sqrt{\frac{t^{(n-1)}}{\varsigma^{(n-1)}}}\left(\varsigma-\varsigma^{(n-1)}\right)+\frac{1}{2}\sqrt{\frac{\varsigma^{(n-1)}}{t^{(n-1)}}}\left(t-t^{(n-1)}\right).$$

As for the non-convex constraint (54), we add another slack variables $\{a_{C,k}\}$ and $\{a_{S,m}\}$ to equivalently reformulate it. Taking the term $R_{C,k}\geq\delta_{C,k}$ in (54) as an example, it can be reformulated as

$$\ln\left(1+a_{C,k}\right)\geq\left(\ln 2\right)\delta_{C,k}=\widetilde{\delta}_{C,k},\forall k \tag{56}$$

$$\frac{\left|\mathbf{g}_{C,k}^H\mathbf{w}_B\right|^2}{\sum_{m=1}^{M}\left|\mathbf{s}_{C,k}^H\mathbf{w}_{S,m}\right|^2+\widetilde{\sigma}_{C,k}^2}\geq a_{C,k},\forall k, \tag{57}$$

where
$$\mathbf{g}_{C,k}^H=\mathbf{v}_{C,k}^H\mathbf{H}_{C,k}\mathbf{\Omega}_{(1,A)},\mathbf{s}_{C,k}^H=\mathbf{v}_{C,k}^H\mathbf{F}_{C,k},$$
$$\widetilde{\sigma}_{C,k}^2=\sum_{l=1}^{L}\left|\mathbf{v}_{C,k}^H\mathbf{Z}_{C,lk}\mathbf{w}_{J,l}\right|^2+\left|\mathbf{v}_{C,k}^H\mathbf{n}_{C,k}\right|^2,$$

Obviously, the constraint (56) can be directly transformed into a tractable one, i.e., $1+a_{C,k}\geq e^{\widetilde{\delta}_{C,k}},\forall k$. Nevertheless, the term $e^{\widetilde{\delta}_{C,k}}$ insides (56) is a generalized non-linear convex program, which leads to the high computational complexity. Thus, by referring to [32], the constraint (56) can be approximated by a series of second order cone (SOC) forms, i.e.,

$$\begin{cases}
1+z_{C,k1}\geq\left\|\left[1-z_{C,k1},2+\widetilde{\delta}_{C,k}\Big/2^{Q-1}\right]^T\right\|, \\
1+z_{C,k2}\geq\left\|\left[1-z_{C,k2},5/3+\widetilde{\delta}_{C,k}\Big/2^{Q}\right]^T\right\|, \\
1+z_{C,k3}\geq\left\|\left[1-z_{C,k3},2z_{C,k1}\right]^T\right\|, \\
z_{C,k4}\geq 19/72+z_{C,k2}+z_{C,k3}/24, \\
1+z_{C,kq}\geq\left\|\left[1-z_{C,kq},2z_{C,k(q-1)}\right]^T\right\|,q=5,\cdots,Q+3, \\
1+z_{C,k(Q+4)}\geq\left\|\left[1-z_{C,k(Q+4)},2z_{C,k(Q+3)}\right]^T\right\|, \\
1+a_{C,k}\geq z_{C,k(Q+4)},\forall k.
\end{cases} \tag{58}$$

where $\{z_{C,kq}\}$ is the introduced slack variables. Next, to handle the non-convexity of constraint (57), we add a positive slack variable $\{\theta_{C,k}\}$ and re-express (57) as the following equivalent form, i.e.,

$$\left|\mathbf{g}_{C,k}^H\mathbf{w}_B\right|^2\geq a_{C,k}\theta_{C,k},\forall k, \tag{59}$$

$$\sum_{m=1}^{M}\left|\mathbf{s}_{C,k}^H\mathbf{w}_{S,m}\right|^2+\widetilde{\sigma}_{C,k}^2\leq\theta_{C,k}. \tag{60}$$

Without loss of generality, since an arbitrary phase rotation of $\mathbf{w}_B$ can be added to make the imaginary part of $\mathbf{g}_{C,k}^H\mathbf{w}_B$ to be zero and it does not change the rate, the constraint (59) can be reformulated as the

$$\Re\left(\mathbf{g}_{C,k}^H\mathbf{w}_B\right)\geq\sqrt{a_{C,k}\theta_{C,k}},\Im\left(\mathbf{g}_{C,k}^H\mathbf{w}_B\right)=0,\forall k, \tag{61}$$

Similar to (55), to tackle the concave term $\sqrt{a_{C,k}\theta_{C,k}}$, we replace it with the first-order Taylor series, and thus constraint (61) can be recast as

$$\Re\left(\mathbf{g}_{C,k}^H\mathbf{w}_B\right)\geq\sqrt{a_{C,k}^{(n-1)}\theta_{C,k}^{(n-1)}}+\frac{1}{2}\sqrt{\frac{a_{C,k}^{(n-1)}}{\theta_{C,k}^{(n-1)}}}\left(\theta_{C,k}-\theta_{C,k}^{(n-1)}\right)$$
$$+\frac{1}{2}\sqrt{\frac{\theta_{C,k}^{(n-1)}}{a_{C,k}^{(n-1)}}}\left(a_{C,k}-a_{C,k}^{(n-1)}\right),\forall k. \tag{62}$$

In terms of the non-convex constraint (60), by introducing the slack variable $\{b_{C,km}\}$ and using the first-order Taylor series expansion, it can be directly converted into the SOC constraints

$$\begin{cases}
\left|\mathbf{s}_{C,k}^H\mathbf{w}_{H,m}\right|\leq b_{C,km},\forall k,m, \\
\frac{\theta_{C,k}+1}{2}\geq\left\|\left[\frac{\theta_{C,k}-1}{2},\{b_{C,km}\},\widetilde{\sigma}_{C,k}\right]^T\right\|,\forall k,
\end{cases} \tag{63}$$

Similar to the abovementioned approximation of the the term $R_{C,k} \geq \delta_{C,k}$ in (54), the other term $R_{S,m} \geq \delta_{S,m}$ of (54) can also be reformulated as

$$\begin{cases} 1 + z_{S,m1} \geq \left\| \left[1 - z_{S,m1}, 2 + \widetilde{\delta}_{S,m} \middle/ 2^{Q-1} \right]^T \right\|, \\ 1 + z_{S,m2} \geq \left\| \left[1 - z_{S,m2}, 5/3 + \widetilde{\delta}_{S,m} \middle/ 2^Q \right]^T \right\|, \\ 1 + z_{S,m3} \geq \left\| \left[1 - z_{S,m3}, 2z_{S,m1} \right]^T \right\|, \\ z_{S,m4} \geq 19/72 + z_{S,m3} + z_{S,m3}/24, \\ 1 + z_{S,mq} \geq \left\| \left[1 - z_{S,m1}, 2z_{S,m(q-1)} \right]^T \right\|, q = 5, \cdots, Q+3, \\ 1 + z_{S,m(Q+4)} \geq \left\| \left[1 - z_{S,m(Q+4)}, 2z_{S,m(Q+3)} \right]^T \right\|, \\ 1 + a_{S,m} \geq z_{S,m(Q+4)}, \forall m, \end{cases}$$
$$(64)$$

$$\Re \left(\mathbf{s}_{S,m}^H \mathbf{w}_{H,m} \right) \geq \sqrt{a_{S,m}^{(n-1)} \theta_{S,m}^{(n-1)}} + \frac{1}{2} \sqrt{\frac{a_{S,m}^{(n-1)}}{\theta_{S,m}^{(n-1)}}} \left(\theta_{S,m} - \theta_{S,m}^{(n-1)} \right)$$
$$+ \frac{1}{2} \sqrt{\frac{\theta_{S,m}^{(n-1)}}{a_{S,m}^{(n-1)}}} \left(a_{S,m} - a_{S,m}^{(n-1)} \right), \forall m, \quad (65)$$

$$\begin{cases} \left| \mathbf{s}_{S,m}^H \mathbf{w}_{H,i} \right| \leq b_{S,mi}, \left| \mathbf{g}_{S,m}^H \mathbf{w}_B \right| \leq c_{S,m}, \forall m, \\ \frac{\theta_{S,m}+1}{2} \geq \left\| \left[\frac{\theta_{S,m}-1}{2}, \{b_{S,mi}\}, \widetilde{\sigma}_{S,m} \right]^T \right\|, i \neq m, \forall m, \end{cases} \quad (66)$$

where $\{z_{S,mq}, a_{S,m}, \theta_{S,m}, b_{S,mi}, c_{S,m}, \delta_{C,k}\}$ are the positive slack variables, and $\mathbf{g}_{S,m}^H = \mathbf{v}_{S,m}^H \mathbf{H}_{S,m} \mathbf{\Omega}_{(1,A)}, \mathbf{s}_{S,m}^H = \mathbf{v}_{S,m}^H \mathbf{F}_{S,m}, \widetilde{\delta}_{S,m} = (\ln 2) \delta_{C,k},$

$$\widetilde{\sigma}_{S,m}^2 = \sum_{l=1}^L \left| \mathbf{v}_{S,m}^H \mathbf{Z}_{S,lm} \mathbf{w}_{J,l} \right|^2 + \left| \mathbf{v}_{S,m}^H \mathbf{n}_{S,m} \right|^2.$$

The non-convexity of constraint (52) can be tackled by adding a new positive slack variable ϑ and decomposed into

$$\sqrt{\varsigma} \geq \vartheta, \quad (67)$$

$$\eta_1 \sum_{m=1}^M \|\mathbf{w}_{S,m}\|^2 + \eta_2 \|\mathbf{w}_B\|^2 + P_S + P_B \leq \sqrt{\varsigma}. \quad (68)$$

Obviously, the constraint (67) and (68) can further be transformed as the following SOC constraints:

$$\begin{cases} \sqrt{\varsigma} \geq \vartheta \Rightarrow \frac{\varsigma+1}{2} \geq \left\| \left[\frac{\varsigma-1}{2}, \vartheta \right]^T \right\|, \\ \|\mathbf{w}_{H,m}\| \leq d_{H,m}, \forall m, \|\mathbf{w}_B\| \leq d_B, \\ \frac{\vartheta+1}{2} \geq \left\| \left[\frac{\vartheta-1}{2}, \{\sqrt{\eta_1} d_{H,m}\}, \sqrt{\eta_2} d_B, \sqrt{P_S}, \sqrt{P_B} \right]^T \right\|, \end{cases} \quad (69)$$

where $\{d_{H,m}\}$ and d_B are the positive slack variables.

Using the above approximations, the original non-convex objective function (19a) and the additional constraints (50c) can be addressed. However, the problem remains non-convex due to the non-convex constraints $(19b)^*$ and $(19c)^*$. First, we convert $(19b)^*$ and $(19c)^*$ into the equivalent forms:

$$\widetilde{\Gamma}_{C,k} \left| \mathbf{g}_{C,k}^H \mathbf{w}_B \right|^2 \geq \sum_{m=1}^M \left| \mathbf{s}_{C,k}^H \mathbf{w}_{H,m} \right|^2 + \widetilde{\sigma}_{C,k}^2, \forall k, \quad (70a)$$

$$\widetilde{\Gamma}_{S,m} \left| \mathbf{s}_{H,m}^H \mathbf{w}_{S,m} \right|^2 \geq \sum_{i \neq m}^M \left| \mathbf{s}_{S,m}^H \mathbf{w}_{H,i} \right|^2 + \left| \mathbf{g}_{S,m}^H \mathbf{w}_B \right|^2 + \widetilde{\sigma}_{S,m}^2, \forall m, \quad (70b)$$

To proceed on, we define a proxy function as follows [33]

$$f(\varpi_{i,j}) = \left| \mathbf{g}_i^H \mathbf{w}_j \right|^2 = \left\| \left[\Re \left(\mathbf{g}_i^H \mathbf{w}_j \right), \Im \left(\mathbf{g}_i^H \mathbf{w}_j \right) \right]^T \right\|^2, \quad (71)$$

where $\varpi_{i,j} = \left[\Re \left(\mathbf{g}_i^H \mathbf{w}_j \right), \Im \left(\mathbf{g}_i^H \mathbf{w}_j \right) \right]^T$. Then, by applying

the first-order Taylor series expansion and considering two most significant terms, we can obtain that

$$f(\varpi_{i,j}) \cong f\left(\varpi_{i,j}^{(n-1)} \right) + 2 \left(\varpi_{i,j}^{(n-1)} \right)^T \left(\varpi_{i,j} - \varpi_{i,j}^{(n-1)} \right). \quad (72)$$

By using (72), each element in the constraints (70) can be transformed into the following linear function:

$$\left| \mathbf{g}_i^H \mathbf{w}_j \right|^2 \cong \left\| \begin{bmatrix} \Re \left(\mathbf{g}_i^H \mathbf{w}_j^{(n-1)} \right) \\ \Im \left(\mathbf{g}_i^H \mathbf{w}_j^{(n-1)} \right) \end{bmatrix} \right\|^2 + 2 \begin{bmatrix} \Re \left(\mathbf{g}_i^H \mathbf{w}_j^{(n-1)} \right) \\ \Im \left(\mathbf{g}_i^H \mathbf{w}_j^{(n-1)} \right) \end{bmatrix}^T$$
$$\times \begin{bmatrix} \Re \left(\mathbf{g}_i^H \mathbf{w}_j \right) - \Re \left(\mathbf{g}_i^H \mathbf{w}_j^{(n-1)} \right) \\ \Im \left(\mathbf{g}_i^H \mathbf{w}_j \right) - \Im \left(\mathbf{g}_i^H \mathbf{w}_j^{(n-1)} \right) \end{bmatrix}. \quad (73)$$

By incorporating all of these approximations, the original problem (50) can be reformulated as

$$\max_{\substack{\mathbf{w}_B, \mathbf{w}_{H,m}, t, \varsigma, \vartheta \{z_{S,mq}\}, \{z_{C,kq}\}, \{a_{C,k}\}, \{\theta_{C,k}\}, \{\delta_{C,k}\}, \\ \{\delta_{S,m}\}, \{b_{C,km}\}, \{a_{S,m}\}, \{\theta_{S,m}\}, \{b_{S,mi}\}, \{c_{S,m}\}, \{d_{H,m}\}, d_B}} t \quad (74)$$

$$s.t. (55), (58), (62) - (66), (69), \overline{(70a)}, \overline{(70b)}, (19f), (50d), (50e),$$

where constraint $\overline{(X)}$ denotes the modified version of (X) by replacing (73) instead of each term in (X). As such, the initial EE-Max problem (50) can be iteratively solved using the convex problem (74), whose convergence can be found in [34]. However, since the initial point $\left\{ \mathbf{w}_B^{(0)}, \mathbf{w}_{H,m}^{(0)}, t^{(0)}, \varsigma^{(0)}, a_{C,k}^{(0)}, \theta_{C,k}^{(0)}, a_{S,m}^{(0)}, \theta_{S,m}^{(0)} \right\}$ is randomly obtained, the convergence and the feasibility of (74) cannot be always generated. To handle this drawback, we use a positive variable ε to judge whether the constraints of (74) are satisfied and obtain the feasible initial point, which is given by

$$\max_{\substack{\varepsilon, \mathbf{w}_B, \mathbf{w}_{H,m}, t, \varsigma, \vartheta \{z_{S,mq}\}, \{z_{C,kq}\}, \{a_{C,k}\}, \{\theta_{C,k}\}, \{\delta_{C,k}\}, \\ \{\delta_{S,m}\}, \{b_{C,km}\}, \{a_{S,m}\}, \{\theta_{S,m}\}, \{b_{S,mi}\}, \{c_{S,m}\}, \{d_{H,m}\}, d_B}} \varepsilon \quad (75)$$

$$s.t. \quad \widehat{(55)}, \widehat{(58)}, \widehat{(62)} - \widehat{(66)}, \widehat{(69)},$$
$$\widehat{(70a)}, \widehat{(70b)}, \widehat{(19f)}, \widehat{(50d)}, \widehat{(50e)},$$

where constraint $\widehat{(X)}$ denotes the modified version of (X) with ε. In particular, the original constraint $f(X) \leq 0$ is replace with $f(X) \leq \varepsilon$. Thus, the feasible initial points $\left\{ \mathbf{w}_B^{(0)}, \mathbf{w}_{H,m}^{(0)}, t^{(0)}, \varsigma^{(0)}, a_{C,k}^{(0)}, \theta_{C,k}^{(0)}, a_{S,m}^{(0)}, \theta_{S,m}^{(0)} \right\}$ can be found by solving (75), whose convergence has been proved in [35].

C. Monotonic Vertex-Update Scheme over $\mathbf{P}_a$

In this subsection, we focus on optimizing the analog precoder $\mathbf{P}_a, \forall a$. Since $\mathbf{P}_a$ does not affect the value of P_{tot}, the initial problem can be transformed into a sum rate maximization problem, which is given by

$$\max_{\mathbf{P}_a} \min_{\Delta_J} \sum_{k=1}^K \mu_{C,k} R_{C,k} + \sum_{m=1}^M \mu_{S,m} R_{S,m} \quad (76)$$

$$s.t. (19b) - (19e), (19g).$$

According to **Definition 3.1** and **Definition 3.2** in [36], the problem (76) maximizes a strictly increasing objective function over $\{R_{C,k}, R_{S,m}\}$, and thus it can be solved by using the outer polyblock block approximation. As such, a novel monotonic vertex-update approach (MVU) is proposed to solve $\mathbf{P}_a, \forall a$. Specifically, we first construct a set of overlapping vertices which contains the the achievable region where the optimal solution lies in. Then, we search for the optimal solution $\{R_{C,k}, R_{S,m}\}$ in the vertices set, and thus

the size of vertices set decreases in an iterative manner until coverage to the optimal solution. Therefore, defining the slack variables $\mathbf{r} = \{r_{C,1}, \cdots, r_{C,K}, r_{S,1}, \cdots, r_{S,M}\}$ to denote the achievable rate $\{R_{C,k}, R_{S,m}\}$, the problem can be recast as

$$\max_{\mathbf{p}_a} \min_{\Delta_J} g(\mathbf{r}) = \sum_{k=1}^{K} \mu_{C,k} r_{C,k} + \sum_{m=1}^{M} \mu_{S,m} r_{S,m} \quad (77)$$

$$s.t.\,(19b) - (19e), (19g),$$

where $g(\mathbf{r})$ denotes the objective function of $\mathbf{r}$. Before utilizing the MUV approach, we also use the discretization method proposed in Section III-B to tackle the CSI uncertainties Δ_J and Δ_E, i.e., (48) and

$$\widetilde{\mathbf{H}}_{E,ra} = \sum_{i=1}^{N_{R1}} \sum_{j=1}^{N_{R2}} \frac{1}{N_R} \overline{\mathbf{h}}_{E,ra}^{(i,j)} \overline{\mathbf{h}}_{E,ra}^{(i,j),H}, \forall r, a, \quad (78)$$

where $\overline{\mathbf{h}}_{E,ra}^{H} = \mathbf{h}_{E,r}^{H} \boldsymbol{\Omega}_{(A,a+1)} \text{diag}(\mathbf{B}_a \boldsymbol{\Omega}_{(a-1,1)} \mathbf{w}_B)$. As such, $\min_{\Delta_J}$ and $\max_{\Delta_E}$ in (77) can be removed. After some mathematical transformations, the optimzation problem on independent $\mathbf{p}_a$ can be rewritten as

$$\max_{\mathbf{p}_a} g(\mathbf{r}) = \sum_{k=1}^{K} \mu_{C,k} r_{C,k} + \sum_{m=1}^{M} \mu_{S,m} r_{S,m} \quad (79a)$$

$$s.t.\,\Re\left(\overline{\mathbf{h}}_{C,ka}^{H} \mathbf{p}_a\right) \geq \sqrt{\beta_{C,k}\left(2^{\widehat{r}_{C,k}} - 1\right)}, \forall k, \quad (79b)$$

$$\left|\overline{\mathbf{h}}_{S,ma}^{H} \mathbf{p}_a\right| \leq \sqrt{\xi_{S,mm}\Big/\left(2^{\widehat{r}_{S,m}} - 1\right) - \widehat{\sigma}_{S,m}^2}, \forall m, \quad (79c)$$

$$\text{Tr}\left\{\widetilde{\mathbf{H}}_{E,ra} \mathbf{P}_a\right\} \leq \widehat{\sigma}_{E,r}^2\left(2^{\Gamma_{B,r}} - 1\right), \forall r, \quad (79d)$$

$$\text{Tr}\left\{\widetilde{\mathbf{H}}_{E,ra} \mathbf{P}_a\right\} \geq \frac{\xi_{E,rm}}{\left(2^{\Gamma_{E,rm}} - 1\right)} - \widetilde{\sigma}_{E,rm}^2, \forall r, m, \quad (79e)$$

$$\left|[\mathbf{p}_a]_i\right| = 1, i = 1, \cdots, N_R, \quad (79f)$$

where $\widehat{r}_{C,k} = \max\{r_{C,k}, \Gamma_{C,k}\}$, $\widehat{r}_{S,m} = \max\{r_{S,m}, \Gamma_{S,m}\}$, $\overline{\mathbf{h}}_{C,ka}^{H} = \mathbf{v}_{C,k}^{H} \mathbf{H}_{C,k} \boldsymbol{\Omega}_{(A,a+1)} \text{diag}(\mathbf{B}_a \boldsymbol{\Omega}_{(a-1,1)} \mathbf{w}_B)$, $\overline{\mathbf{h}}_{S,ma}^{H} = \mathbf{v}_{S,m}^{H} \mathbf{H}_{S,m} \boldsymbol{\Omega}_{(A,a+1)} \text{diag}(\mathbf{B}_a \boldsymbol{\Omega}_{(a-1,1)} \mathbf{w}_B)$, $\xi_{S,mi} = \left|\mathbf{v}_{S,m}^{H} \mathbf{F}_{S,m} \mathbf{w}_{S,i}\right|^2, \forall i, \xi_{E,rm} = \mathbf{w}_{S,m}^{H} \widetilde{\mathbf{F}}_{E,r} \mathbf{w}_{S,m}$, $\widehat{\sigma}_{S,m}^2 = \sum_{i=1,i\neq m}^{M} \xi_{S,mi} + \widetilde{\sigma}_{S,m}^2, \widetilde{\sigma}_{E,rm}^2 = \sum_{i=1,i\neq m}^{M} \xi_{E,ri} + \sigma_{E,r}^2$, $\widehat{\sigma}_{E,r}^2 = \sum_{m=1}^{M} \mathbf{w}_{S,m}^{H} \widetilde{\mathbf{F}}_{E,r} \mathbf{w}_{S,m} + \sigma_{E,r}^2$, $\mathbf{P}_a = \mathbf{p}_a^{(n-1)} \mathbf{p}_a^{H} + \mathbf{p}_a \mathbf{p}_a^{(n-1),H} - \mathbf{p}_a^{(n-1)} \mathbf{p}_a^{(n-1),H}$. Note that (79b) is obtained by adding an arbitrary phase rotation which is similar to (61), and $\mathbf{P}_a$ are obtained by the first-order Taylor series.

Then, the MVU approach is adopted to solve the optimal $\{R_{C,k}, R_{S,m}\}$ and $\mathbf{p}_a$ in (79). Here, we use the MVU approach to obtain $\mathbf{p}_1 \to \mathbf{p}_a \to \mathbf{p}_A$ in an iterative manner. Firstly, we define the Pareto boundary and the vertex set.

Definition 1: The upper bound of the defined rate region is called Pareto boundary, which is constituted by $\{R_{C,k}, R_{S,m}\}$.

Definition 2: Given $\mathbf{u} \leq \mathbf{v} \in \mathbb{R}_+^{K+M}$, the hyper rectangle $[\mathbf{u}, \mathbf{v}] = \{\mathbf{x} \mid \mathbf{u} \leq \mathbf{x} \leq \mathbf{v}\}$ is defined as the vertex set.

We initialize a vertex set $\mathbb{O} = [\mathbf{u}^{(0)}, \mathbf{v}^{(0)}]$, where the minimal rate of each user in $\{R_{C,k}, R_{S,m}\}$ is obtained by the rate threshold in (19b) and (19c), which is expressed as $\Gamma_{C,k}$ and $\Gamma_{S,m}$. And the maximal value of $\{R_{C,k}, R_{S,m}\}$ is calculated as

$\log_2\left(1 + N_R\left\|\overline{\mathbf{h}}_{C,ka}^{H}\right\|^2\Big/\beta_{C,k}\right)$ or $\log_2\left(1 + \xi_{S,mm}/\widehat{\sigma}_{S,m}^2\right)$, which is obtained by letting BS/HAP only serves one user with maximum transmit power and ignoring the interference from HAP/BS. Moreover, we use the Cauchy-Schwarz inequality to obtain the upper bound of desired signal power, i.e., $\left|\overline{\mathbf{h}}_{C,ka}^{H} \mathbf{p}_a\right|^2 \leq \|\mathbf{p}_a\|^2 \left\|\overline{\mathbf{h}}_{C,ka}^{H}\right\|^2 = N_R\left\|\overline{\mathbf{h}}_{C,ka}^{H}\right\|^2$. Thus, the initial upper and lower bounds of $g(\mathbf{r})$ is given by $g_{\max} = g(\mathbf{v}^{(0)})$ and $g_{\min} = g(\mathbf{u}^{(0)})$.

Clearly, the optimal solution lies in $\mathbb{O}$. Thus, we first choose a vertex set $[\mathbf{u}^{(n)}, \mathbf{v}^{(n)}]$ insides $\mathbb{O}$ at the n-th iteration, where $g(\mathbf{u}^{(n)}) = g_{\min}$ and $g(\mathbf{v}^{(n)}) = g_{\max}$. Then, we define $l_{\mathbf{uv}}$ as the line that connects the two vertices $\mathbf{u}^{(n)}$ and $\mathbf{v}^{(n)}$, and search along line $l_{\mathbf{uv}}$ for the optimal solution. In particular, any point $\boldsymbol{\chi}$ on $l_{\mathbf{uv}}$ with $R_{\text{sum}} = g(\boldsymbol{\chi})$ can be expressed as

$$l_{\mathbf{uv}} : \boldsymbol{\chi} = \mathbf{u}^{(n)} + \left(\mathbf{u}^{(n)} - \mathbf{v}^{(n)}\right) \frac{R_{\text{sum}} - g_{\min}}{g\left(\mathbf{u}^{(n)} - \mathbf{v}^{(n)}\right)}. \quad (80)$$

Since $\mathbf{u}^{(n)}$ may be infeasible to the problem (79), we should check the feasibility of vertex $\mathbf{u}^{(n)}$ at first. Given $\{r_{C,k}, r_{S,m}\} = \mathbf{u}^{(n)}$, the feasibility-check problem can be formulated as

$$\max_{\mathbf{p}_a} 0 \; s.t.\,(79b) - (79f). \quad (81)$$

However, the problem remains non-convex due to the non-convex strict equality (79f). Thus, we propose a P-CCP method to optimize (81). Specifically, we introcuce two real positive vectors $\boldsymbol{\tau}_a = [\tau_{a,1}, \cdots, \tau_{a,N_R}]^T$ and $\boldsymbol{\eta}_a = [\eta_{a,1}, \cdots, \eta_{a,N_R}]^T$ to convert constraint (79f) into the following form:

$$1 - \tau_{a,i} \leq |p_{a,i}|^2 \leq 1 + \eta_{a,i}, \forall i. \quad (82)$$

Note that the left inequality in (82) is still non-convex, and thus we approximate it as $2\text{Re}\left\{p_{a,i}^{(n-1),*} p_{a,i}\right\} - \left|p_{a,i}^{(n-1)}\right|^2 \geq 1 - \tau_{a,i}$. Moreover, to guarantee that the slack variables can converge to zero, $\sum_{i=1}^{N_R} \tau_{a,i} + \sum_{i=1}^{N_R} \eta_{a,i}$ is introcuced to the objective function of (81) based on the concept of P-CCP, which is penalized by a penalty parameter γ [37]. As such, problem (81) can be reconstructed as

$$\max_{\mathbf{p}_a, \boldsymbol{\tau}_a, \boldsymbol{\eta}_a} -\gamma\left(\sum_{i=1}^{N_R} \tau_{a,i} + \sum_{i=1}^{N_R} \eta_{a,i}\right) \quad (83a)$$

$$s.t.\,(79b) - (79e), |p_{a,i}|^2 \leq 1 + \eta_{a,i}, \forall i, \quad (83b)$$

$$2\text{Re}\left\{p_{a,i}^{(n-1),*} p_{a,i}\right\} - \left|p_{a,i}^{(n-1)}\right|^2 \geq 1 - \tau_{a,i}, \forall i. \quad (83c)$$

Here, we refresh γ in each iteration, and it is bounded by the upper limit $\gamma_{\max}$. According to [37], problem (83) is always guaranteed to converge, where the proof can be found in [37] or [19]. Hence, with given γ, the feasibility and optimal solution to (79) can be obtained by solving (83).

If $\mathbf{u}^{(n)}$ is feasible to problem (79), we utilize Fibonacci search method along line $l_{\mathbf{uv}}$ to obtain the intersection point $\boldsymbol{\rho}^{(n)}$ on the Pareto boundary [38], which is is omitted for brevity. Thus, the lower bound of $g(\mathbf{r})$ is updated to $g_{\min} = g(\boldsymbol{\rho}^{(n)})$. Next, in order to improve the the upper bound of $g(\mathbf{r})$, we update the vertex set by using the following method. Based on the intersection point $\boldsymbol{\rho}^{(n)}$, $K + M$ new upper vertices adjacent to $\mathbf{v}^{(n)}$ can be expressed as

$$\mathbf{v}^{(n),i} = \mathbf{v}^{(n)} - \left(v_i^{(n)} - \rho_i^{(n)}\right)\mathbf{e}_i, i = 1, \cdots, K+M, \quad (84)$$

where $\mathbf{v}^{(n),i}$ is the i-th new vertex generated at the n-th iteration, $v_i^{(n)}$ and $\rho_i^{(n)}$ denotes the i-th element of $\mathbf{v}^{(n)}$ and

$\boldsymbol{\rho}^{(n)}$. Then, the corresponding lower vertices adjacent to $\mathbf{u}^{(n)}$ can be obtained by

$$\mathbf{u}^{(n),i} = \begin{cases} \mathbf{u}^{(n)}, i = 1, \\ \mathbf{u}^{(n),i-1} + \left(\rho_{i-1}^{(n)} - u_{i-1}^{(n)}\right)\mathbf{e}_{i-1}, i > 1. \end{cases} \quad (85)$$

As such, the new new vertex set can be updated to

$$\mathbb{O} = \mathbb{O} \Big/ \left[\mathbf{u}^{(n)}, \mathbf{v}^{(n)}\right] \bigcup_{i=1,\cdots,K+M} \left[\mathbf{u}^{(n),i}, \mathbf{v}^{(n),i}\right]. \quad (86)$$

Since the intersection point $\boldsymbol{\rho}^{(n)}$ is close to the Parato boundary, the updated vertex set also contains the optimal solution, and the size of new vertex set becomes smaller. The illustration of each iteration is shown in Fig. 4. Then, the whole iterative algorithm can terminate to the optimal $\{R_{C,k}, R_{S,m}\}$. Finally, the optimal $\mathbf{p}_a$ can be obtained by solving (83).

(a) $(n-1)$-th iteration. (b) n-th iteration.
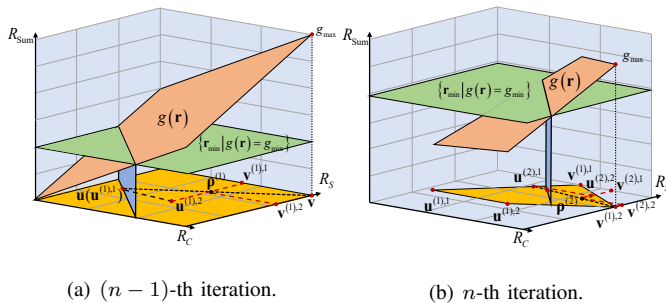
Fig. 4: Illustration of each iteration $K + M = 2$.

Remark 1: Different from the outer polyblock block approximation in [36] which optimizes the target in whole achievable rate region, the MUV approach only maintains the optimal solutions and update the achievable rate region in each iteration, and thus it can be regarded as more efficient polyblock. On the other hand, as compared to the improved polyblock scheme in [9] which use the bisection method to search for the Pareto boundary, the MVU approach utilize the Fibonacci search method to obtain the Pareto boundary, and thus the lower computational time can be achieved due to the no use of division [38]. Besides, since we directly use the point $\mathbf{u}^{\min}$ to compute the intersection point, the size of vertex set of MUV approach is shortened than the polyblock scheme in [9]. Above all, a novel feasibility check scheme combined with SCA, Taylor expansion, and P-CCP is proposed to transform the beamforming matrix into a linear formulation of beamforming vector, avoiding the process of semidefinite relaxation (SDR), which may leads to suboptimal or even far from optimal one. In the nutshell, the proposed MVU approach is a more efficient polyblock than that of [9] and [36].

IV. SIMULATION RESULTS

In this section, numerical simulations are presented to illustrate the superiority and validity of the proposed architectures and algorithms. Here, we consider a scenario of $K = 2$ CUs, $M = 2$ ESs, $L = 2$ jammers, and $R = 3$ Eves. The achievable rate thresholds of the ESs and CUs are set as $\Gamma_{C,k} = \Gamma_{S,m} = 2$ bps/Hz, and the wiretap rate targets are set as $\Gamma_{B,r} = \Gamma_{E,rm} = 0.5$ bps/Hz. For simplicity, the weighted factor of user rate are set as $\mu_{C,k} = \mu_{S,m} = 1/(K+M)$. The

number of jammer's antennas is set as $N_J = 8 \times 8$, and the jamming beamforming are obtained by using the beamforming algorithm in [22], whose main lobe points to the nearest user. The total power consumption of the full-digital, the fully-connected, and sub-connected architecture are shown in [23], and is omitted for simplicity. In addition, the RF chains, the power amplifiers, the phase shifters, the RIS unit, and the baseband processor power consumption of the BS and HAP are set as $P_{rc} = 100$ mW, $P_a = 30$ mW, $P_s = 10$ mW, $P_{ris} = 5$ mW, and $P_{bb} = P_{hb} = 400$ mW, respectively [14]. The carrier frequency of all network is 5.8 GHz, and the noise power variance is set as $\sigma_{C,k}^2 = \sigma_{S,m}^2 = \sigma_{E,r}^2 = 10^{-8}$. We set the inefficiency and the maximum power of BS and HAP as $\eta_1 = \eta_2 = 1.25$ and $P_{B,max} = P_{H,max} = 0.5$ W, respectively. Here, we compare the performance of proposed beamforming (BF) scheme and architecture with that of the following schemes and architectures: (1) **SDR-based multi-layer BF scheme**: the MVU approach combined with the SDR method is adopted to solve problem (77) instead of that with proposed P-CCP; (2) **SCA-based multi-layer BF scheme**: SCA method is utilized to transform the sum rate maximization problem (76) into a convex iterative one; (3) **Proposed single-layer BF scheme**: single-layer RIS-assisted architecture is adopted at BS side, and the proposed algorithm is used to solve the single-layer EE maximization problem; (4) **Fully-connected BF scheme**: the proposed algorithm with fully-connected architecture at BS; (5) **Sub-connected BF scheme**: the proposed algorithm with sub-connected architecture at BS.

Fig. 5 shows the radiation and received beampattern of different architectures and compare the quality of the beam by comparing their sidelobes and mainlobes. Here, we set $\Delta_E = \Delta_J = 2°$, $p_J = 1$ W, $N_{RF} = 4$, and $N_R = N_H = 8 \times 8$. As we can observe, the mainlobes of all the beampatterns point to the desired target with a value of at least -1 dB, and the nulls can be accurately generated at the region of undesired targets under the CSI imperfection. Specifically, two mainlobes of the RIS-aided beampattern point to two CUs, while the received SINR of the Eves and ESs are limited at the required thresholds. Meanwhile, as illustrated in Fig. 5 (f), both the jamming signals transmitted by two jammers and the interference leakaged by HAP are nullified, and thus only the desired signal quality can be improved at the receiver. On the other hand, compared to single-layer RIS-assisted scheme, the multi-layer one has a higher mainlobe to sidelobe ratio and beam resolution, which is due to the new DoF in amplitude terms caused by the additional layer. Our findings verify that both the multi-layer RIS-assisted beamforming scheme and the received beamforming scheme can efficiently improve the received signal quality at the intended users, suppress the signal leakage at unintended users and simultaneously nullify the undesired signal in the channel uncertainty region.

Fig. 6 depicts the EE versus the number of received antennas N_C and N_S for different algorithms and architectures. It can see that EE of all the schemes can achieve the maximum at $N_C = N_S = 4 \times 4$, which can be explained by the reason that the beam resolution generated by 4×4 geometry can accurately nullify the jamming and interference with the lowest circuit power consumption. This phenomenon further confirms
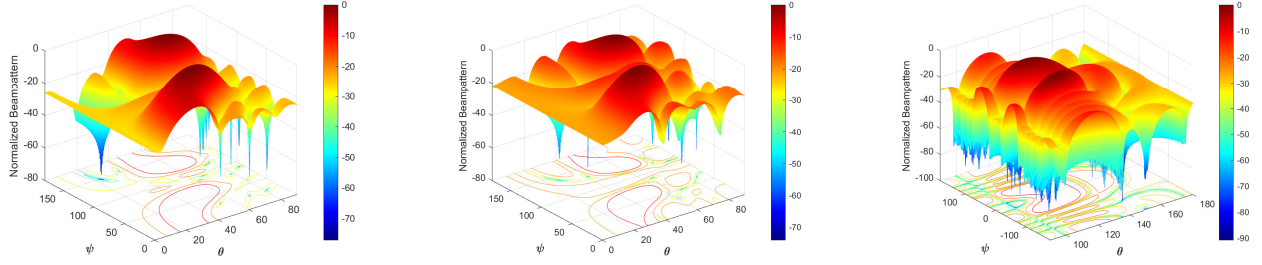
(a) 3D vision of multi-layer RIS-assisted BF $\Delta_E = 2°$.　(b) 3D vision of single-layer RIS-assisted BF $\Delta_E = 2°$.　(c) 3D vision of CU's received BF $\mathbf{v}_{C,2}$ $\Delta_J = 2°$.
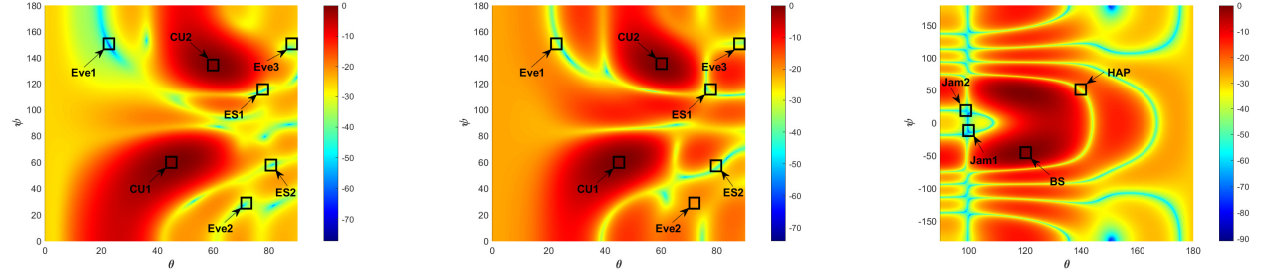
(d) 2D vision of multi-layer RIS-assisted BF $\Delta_E = 2°$.　(e) 2D vision of single-layer RIS-assisted BF $\Delta_E = 2°$.　(f) 2D vision of CU's received BF $\mathbf{v}_{C,2}$ $\Delta_J = 2°$.
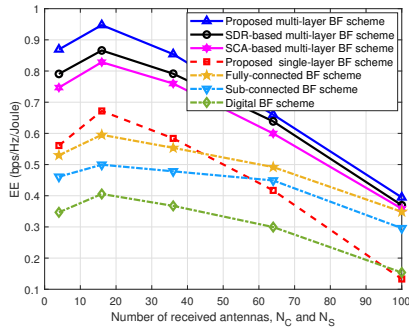
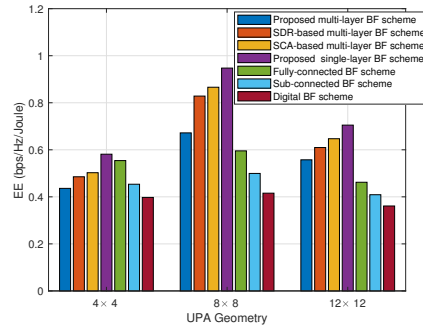Fig. 5: Radiation beampattern with different architectures

Fig. 6: EE versus N_C and N_S
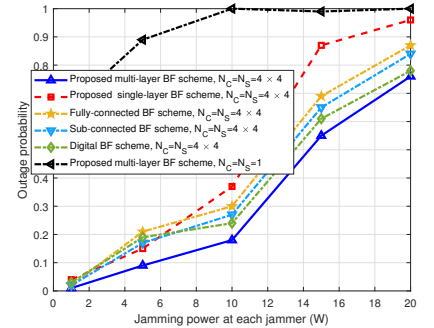
Fig. 7: EE versus N_R

Fig. 8: Outage probability versus p_J.

the validity of our proposed received BF design. Besides, we can also observe that the EE performance of the RIS-assisted architectures is more unstable and even lower than that of three typical architectures when $N_C = N_S > 6 \times 6$. This is because the power consumption of RIS-assisted architectures is very low so that the total power consumption of proposed architecture is dominated by that of receiver. Furthermore, when $N_C = N_S = 4 \times 4$, the proposed multi-layer BF scheme is enhanced by 0.0814 and 0.1190 bps/Hz/Joule in comparison with SDR-based BF scheme and SCA-based BF scheme, respectively, which verifies the superiority of our proposed optimization framework. In addition, in terms of EE, our proposed multi-layer architecture always outperforms other architectures, which demonstrates that our proposed architecture can achieve efficient and secure communications.

The EE versus the transmitter UPA geometry N_R is illustrate in Fig. 7, with $N_{RF} = 4$, $N_H = 8 \times 8$, $N_C = N_S = 4 \times 4$, $p_J = 1$ W, and $\Delta_E = \Delta_J = 2°$. It can be observed that the EE increases as N_R increases from

4×4 to 8×8, this because increasing N_R can significantly improve the DoF and diversity. Besides, the difference in EE between the multi-layer RIS-assisted architecture and other four architectures becomes larger. This can be explained by two reasons. First, as N_R increases, the power distribution of single-layer architecture become more non-uniform, but the multi-layer architecture can balance it (see Fig. 2), so that the performance gap between the single-layer architecture and the multi-layer one becomes larger. Second, compared with three typical architectures which are composed of many phase shifters and power amplifiers, the multi-layer architecture has much lower power consumption, and thus the EE difference between them increases as increasing N_R. Moreover, it is noted that increasing N_R from 8×8 to 12×12 can raise the beam resolution such that the spectral efficiency is slightly improved, however, it also increase the power consumption and, in turn, degrades the EE performance. In Fig. 8, the outage probability (OP) versus the jamming power at each jammer p_J is shown. Obviously, the proposed BF scheme with omnidi-

rectional single-antenna at users, i.e., $N_C = N_S = 1$, achieves the highest OP, verifying the serious threat of the jammers and the importance of designing received BF. Meanwhile, the OP of proposed multi-layer BF scheme with $N_C = N_S = 4 \times 4$ is lower than other four benchmark schemes. This is because the additional layer can boost and partially control the amplitude of the signal, such that the OP performance is enhanced.
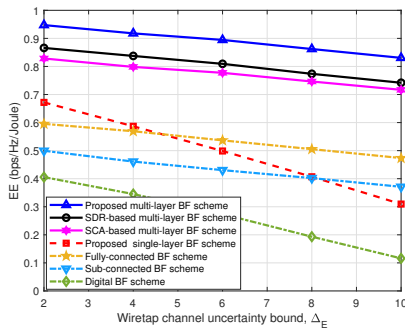
(a) EE versus Δ_E with $\Delta_J = 2°$
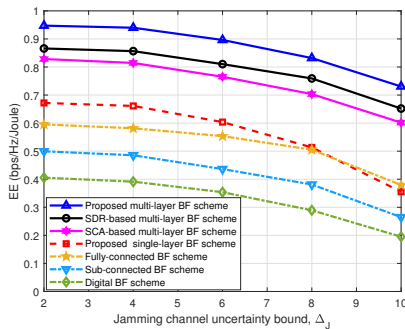
(b) EE versus Δ_J with $\Delta_E = 2°$

Fig. 9: EE versus channel uncertainty Δ.

Fig. 9 presents EE versus the channel uncertainty bound Δ. We assume $N_R = 8 \times 8$, and the other parameters are the same as those in Fig. 7. As expected, the larger channel uncertainty region is, the lower EE obtained. In addition, due to the non-uniform power distribution, the performance decrease speed of single-layer BF scheme is faster than that of other schemes, especially with wiretap channel uncertainty bound Δ_E, verifying that the proposed multi-layer BF scheme has stronger robustness. It can be also seen that when the jamming channel uncertainty bound Δ_J becomes larger, the performance decrease speed of all the BF schemes becomes faster, this is because the jamming signal cannot be accurately nullified as Δ_J increases such that the received jamming power is enhanced. Thus, we can conclude that Δ_J has larger negative effect on the performance as compared to Δ_E.

V. CONCLUSIONS

In this paper, we investigated a novel energy-efficient hybrid beamforming design in the presence of simultaneous jamming and eavesdropping attacks in the RIS-assisted secure ITAN. Considering only the imperfect AoA/AoD is available, and employing multi-layer RIS-assisted transmitter at the BS, we

solved the energy efficiency maximization problem to obtain user's received precoder, BS/HAP's digital precoder, and multi-layer RIS analog precoder, while meeting the desired rate target and wiretap rate requirements. Specifically, a sequential optimization framework was developed by leveraging the heuristic beamforming scheme using the characteristic of convex hull, the iterative SCA approach, and the MVU combined with the P-CCP. The advantage of proposed energy-efficient hybrid beamforming comes from the low power consumption and the additional DoF in amplitude generated by multi-layer architecture. Numerical results confirmed the validity and efficiency of the developed optimization framework and architecture. Our proposed framework and architecture can provide an effective solution to enhance the EE and security of the secure ITAN as well as the extended systems.

APPENDIX A
PROOF OF PROPOSITION 1

Here, we take the derivation of max-min problem (28) as an example. Since the $\Psi_{C,k}$ is the convex hull of $\Psi_{C,k}$, we can obtain $\Lambda_{C,k} \subset \Psi_{C,k}, \forall k$, and then $\max\limits_{\Psi_{C,lk} \subset \Lambda_{C,k}} \sum\limits_{l=1}^{L} \widehat{p}_{J,l} \Psi_{C,lk} \leq \max\limits_{\Psi_{C,lk} \subset \Psi_{C,k}} \sum\limits_{l=1}^{L} \widehat{p}_{J,l} \Psi_{C,lk}$ can be achieved, which leads to

$$\min_{\Lambda_{C,k}} \frac{\mathbf{v}_{C,k}^H \mathbf{A}_{C,k} \mathbf{v}_{C,k}}{\mathbf{v}_{C,k}^H \mathbf{D}_{C,k} \mathbf{v}_{C,k}} \geq \min_{\Psi_{C,k}} \frac{\mathbf{v}_{C,k}^H \mathbf{A}_{C,k} \mathbf{v}_{C,k}}{\mathbf{v}_{C,k}^H \mathbf{D}_{C,k} \mathbf{v}_{C,k}}. \quad (A1)$$

Meanwhile, according to the characteristic of convex hull and using the defination (26), for $\forall \Psi_{C,lk} \subset \Psi_{C,k}$, the term $\mathbf{v}_{C,k}^H \Psi_{C,lk} \mathbf{v}_{C,k}$ insides $\mathbf{v}_{C,k}^H \mathbf{D}_{C,k} \mathbf{v}_{C,k}$ can be decomposed as
$$\mathbf{v}_{C,k}^H \Psi_{C,lk} \mathbf{v}_{C,k} = \mathbf{v}_{C,k}^H (\alpha_{C,lk1} \Psi_{C,lk1} + \cdots + \alpha_{C,lkQ_{C,k}} \Psi_{C,lkQ_{C,k}}) \mathbf{v}_{C,k}$$
$$= \alpha_{C,lk1} \mathbf{v}_{C,k}^H \Psi_{C,lk1} \mathbf{v}_{C,k} + \cdots$$
$$+ \alpha_{C,lkQ_{C,k}} \mathbf{v}_{C,k}^H \Psi_{C,lkQ_{C,k}} \mathbf{v}_{C,k}, \quad (A2)$$

Due to the fact that $\forall \Psi_{C,lk} \subset \Psi_{C,k} = \left\{ \sum\limits_{i=1}^{Q_{C,k}} \alpha_{C,lki} \Psi_{C,lki} \middle| \sum\limits_{i=1}^{Q_{C,k}} \alpha_{C,lki} = 1, \alpha_{C,lki} \geq 0, \forall l \right\}$, there must exist a $\Psi_{C,lkq} \subset \Lambda_{C,k}$ satisfying

$$\frac{\mathbf{v}_{C,k}^H \Psi_{C,lkq} \mathbf{v}_{C,k}}{\mathbf{v}_{C,k}^H \mathbf{A}_{C,k} \mathbf{v}_{C,k}} \geq \frac{\mathbf{v}_{C,k}^H \Psi_{C,lk} \mathbf{v}_{C,k}}{\mathbf{v}_{C,k}^H \mathbf{A}_{C,k} \mathbf{v}_{C,k}}. \quad (A3)$$

As such, we can find a $\Psi_{C,lkq} \subset \Lambda_{C,k}$, which results in

$$\min_{\Lambda_{C,k}} \frac{\mathbf{v}_{C,k}^H \mathbf{A}_{C,k} \mathbf{v}_{C,k}}{\mathbf{v}_{C,k}^H \mathbf{D}_{C,k} \mathbf{v}_{C,k}} \leq \min_{\Psi_{C,k}} \frac{\mathbf{v}_{C,k}^H \mathbf{A}_{C,k} \mathbf{v}_{C,k}}{\mathbf{v}_{C,k}^H \mathbf{D}_{C,k} \mathbf{v}_{C,k}}. \quad (A4)$$

By combining (A1) and (A4), the proof to (28) is completed. Note that the proof to (29) is similar to the abovementioned proof to (28), and thus is omitted here for simplicity

Hence, the proof is completed. ∎

APPENDIX B
PROOF OF PROPOSITION 2

Here, we also take the derivation of max-min problem (30) as an example. To prove **Proposition 2**, the following defination is presented for later derivation, which is given by

$$f(\mathbf{v}_{C,k}, \Psi_{C,lk}) = \frac{\mathbf{v}_{C,k}^H \mathbf{A}_{C,k} \mathbf{v}_{C,k}}{\mathbf{v}_{C,k}^H \mathbf{D}_{C,k} \mathbf{v}_{C,k}} \triangleq \frac{\mathrm{Tr}\{\mathbf{A}_{C,k} \mathbf{V}_{C,k}\}}{\mathrm{Tr}\{\mathbf{D}_{C,k} \mathbf{V}_{C,k}\}}, \quad (A5)$$

where $\mathbf{V}_{C,k} = \mathbf{v}_{C,k} \mathbf{v}_{C,k}^H$ satisfying $\mathrm{rank}(\mathbf{V}_{C,k}) = 1$. Note that $\Psi_{C,lk}$ is a convex set, and thus $f(\mathbf{V}_{C,k}, \Psi_{C,lk})$ is a convex

function with respect to $\boldsymbol{\Psi}_{C,lk} \in \Psi_{C,k}$. By reffering to [39], there must exist a saddle point $\left(\mathbf{V}_{C,k}^*, \boldsymbol{\Psi}_{C,lk}^*\right)$ satisfying

$$f\left(\mathbf{V}_{C,k}, \boldsymbol{\Psi}_{C,lk}^*\right) \leq f\left(\mathbf{V}_{C,k}^*, \boldsymbol{\Psi}_{C,lk}^*\right) \leq f\left(\mathbf{V}_{C,k}^*, \boldsymbol{\Psi}_{C,lk}\right),$$
$$\forall \mathbf{V}_{C,k}, \boldsymbol{\Psi}_{C,lk} \in \Psi_{C,k}, \quad \text{(A6)}$$

Then, according to the saddle point property in the minimax theory [39], we can obtain that

$$f\left(\mathbf{V}_{C,k}^*, \boldsymbol{\Psi}_{C,lk}^*\right) = \max_{\mathbf{V}_{C,k}} \min_{\Psi_{C,k}} f\left(\mathbf{V}_{C,k}, \boldsymbol{\Psi}_{C,lk}\right)$$
$$= \min_{\Psi_{C,k}} \max_{\mathbf{V}_{C,k}} f\left(\mathbf{V}_{C,k}, \boldsymbol{\Psi}_{C,lk}\right). \quad \text{(A7)}$$

The equation (A7) suggests that the max-min problem are equivalent to the min-max one, and thus both have the same optimal solution at the saddle point $\left(\mathbf{V}_{C,k}^*, \boldsymbol{\Psi}_{C,lk}^*\right)$. As such, we can get

$$\max_{\mathbf{V}_{C,k}} \min_{\Psi_{C,k}} \frac{\mathrm{Tr}\left\{\mathbf{A}_{C,k}\mathbf{V}_{C,k}\right\}}{\mathrm{Tr}\left\{\mathbf{D}_{C,k}\mathbf{V}_{C,k}\right\}} = \min_{\Psi_{C,k}} \max_{\mathbf{V}_{C,k}} \frac{\mathrm{Tr}\left\{\mathbf{A}_{C,k}\mathbf{V}_{C,k}\right\}}{\mathrm{Tr}\left\{\mathbf{D}_{C,k}\mathbf{V}_{C,k}\right\}}. \quad \text{(A8)}$$

Replacing $\mathbf{V}_{C,k}$ by $\mathbf{v}_{C,k}$, we can transform (A7) into (30). Similar to the proof to (30), the the proof to (31) can obtained, and thus is omitted here for simplicity.

Hence, the proof is completed. ∎

APPENDIX C
PROOF OF PROPOSITION 3

For simplicity, we still take the derivation of (38) as an example. By denoting $\eta = \left\|\overline{\mathbf{D}}_{C,k}\right\|^2$, it can be observed that

$$\overline{\mathbf{D}}_{C,k}^{\dagger}\mathbf{a}_{C,k}\mathbf{a}_{C,k}^{H}\mathbf{v}_{C,k} = \overline{\mathbf{D}}_{C,k}^{\dagger}\mathbf{a}_{C,k}\left(\mathbf{a}_{C,k}^{H}\frac{1}{\sqrt{\eta}}\overline{\mathbf{D}}_{C,k}^{\dagger}\mathbf{a}_{C,k}\right)$$
$$= \left(\mathbf{a}_{C,k}^{H}\overline{\mathbf{D}}_{C,k}^{\dagger}\mathbf{a}_{C,k}\right)\frac{1}{\sqrt{\eta}}\overline{\mathbf{D}}_{C,k}^{\dagger}\mathbf{a}_{C,k}$$
$$= \lambda_1\mathbf{v}_{C,k}, \quad \text{(A9)}$$

where $\lambda_1 = \mathbf{a}_{C,k}^{H}\overline{\mathbf{D}}_{C,k}^{\dagger}\mathbf{a}_{C,k} > 0$. It suggests that $\mathbf{v}_{C,k}$ is an eigenvector of $\overline{\mathbf{D}}_{C,k}^{\dagger}\mathbf{A}_{C,k}$.

Besides, according to the matrix rank property, we can obtain

$$\mathrm{rank}\left(\overline{\mathbf{D}}_{C,k}^{\dagger}\mathbf{A}_{C,k}\right) \leq \min\left\{\mathrm{rank}\left(\mathbf{A}_{C,k}\right), \mathrm{rank}\left(\overline{\mathbf{D}}_{C,k}^{\dagger}\right)\right\}$$
$$\leq \mathrm{rank}\left(\mathbf{A}_{C,k}\right) = 1. \quad \text{(A10)}$$

Moreover, since $\overline{\mathbf{D}}_{C,k}^{\dagger}\mathbf{A}_{C,k}$ is a non-zero matrix, we get $\mathrm{rank}\left(\overline{\mathbf{D}}_{C,k}^{\dagger}\mathbf{A}_{C,k}\right) = 1$. As such, $\mathbf{v}_{C,k}$ is the only eigenvector of $\overline{\mathbf{D}}_{C,k}^{\dagger}\mathbf{A}_{C,k}$ corresponding to its maximal eigenvalue. Similar to the proof to (38), the the proof to (39) can obtained, and thus is omitted here for simplicity.

Hence, the proof is completed. ∎

REFERENCES

[1] A. Mohammed, A. Mehmood, F.-N. Pavlidou, and M. Mohorcic, "The role of high-altitude platforms (haps) in the global wireless connectivity," *Proc. IEEE*, vol. 99, no. 11, pp. 1939–1953, 2011.

[2] P. G. Sudheesh, M. Mozaffari, M. Magarini, W. Saad, and P. Muthuchidambaranathan, "Sum-rate analysis for high altitude platform (hap) drones with tethered balloon relay," *IEEE Commun. Lett.*, vol. 22, no. 6, pp. 1240–1243, 2018.

[3] X. Cao, P. Yang, M. Alzenad, X. Xi, D. Wu, and H. Yanikomeroglu, "Airborne communication networks: A survey," *IEEE J. Sel. Areas Commun.*, vol. 36, no. 9, pp. 1907–1926, 2018.

[4] A. Alsharoa and M.-S. Alouini, "Improvement of the global connectivity using integrated satellite-airborne-terrestrial networks with resource optimization," *IEEE Trans. Wireless Commun.*, vol. 19, no. 8, pp. 5088–5100, 2020.

[5] Q. Huang, M. Lin, W.-P. Zhu, J. Cheng, and M.-S. Alouini, "Uplink massive access in mixed rf/fso satellite-aerial-terrestrial networks," *IEEE Trans. Commun.*, vol. 69, no. 4, pp. 2413–2426, 2021.

[6] Y. Wu, B. Wang, K. J. R. Liu, and T. C. Clancy, "Anti-jamming games in multi-channel cognitive radio networks," *IEEE J. Sel. Areas Commun.*, vol. 30, no. 1, pp. 4–15, 2012.

[7] Q. Spencer, A. Swindlehurst, and M. Haardt, "Zero-forcing methods for downlink spatial multiplexing in multiuser MIMO channels," *IEEE Trans. Signal Process.*, vol. 52, no. 2, pp. 461–471, 2004.

[8] M. Lin, Z. Lin, W.-P. Zhu, and J.-B. Wang, "Joint beamforming for secure communication in cognitive satellite terrestrial networks," *IEEE J. Sel. Areas Commun.*, vol. 36, no. 5, pp. 1017–1029, 2018.

[9] Z. Lin, M. Lin, Y. Huang, T. d. Cola, and W.-P. Zhu, "Robust multi-objective beamforming for integrated satellite and high altitude platform network with imperfect channel state information," *IEEE Trans. Signal Process.*, vol. 67, no. 24, pp. 6384–6396, 2019.

[10] Y. Sun, D. W. K. Ng, J. Zhu, and R. Schober, "Robust and secure resource allocation for full-duplex MISO multicarrier NOMA systems," *IEEE Trans. Commun.*, vol. 66, no. 9, pp. 4119–4137, 2018.

[11] K. An, M. Lin, J. Ouyang, and W.-P. Zhu, "Secure transmission in cognitive satellite terrestrial networks," *IEEE J. Sel. Areas Commun.*, vol. 34, no. 11, pp. 3025–3037, 2016.

[12] Y. Lu, K. Xiong, P. Fan, Z. Ding, Z. Zhong, and K. B. Letaief, "Global energy efficiency in secure MISO SWIPT systems with non-linear power-splitting EH model," *IEEE J. Sel. Areas Commun.*, vol. 37, no. 1, pp. 216–232, 2019.

[13] Q. Huang, M. Lin, J.-B. Wang, T. A. Tsiftsis, and J. Wang, "Energy efficient beamforming schemes for satellite-aerial-terrestrial networks," *IEEE Trans. Commun.*, vol. 68, no. 6, pp. 3863–3875, 2020.

[14] V. Jamali, A. M. Tulino, G. Fischer, R. R. Mller, and R. Schober, "Intelligent surface-aided transmitter architectures for millimeter-wave ultra massive MIMO systems," *IEEE Open J. Commun. Society*, vol. 2, pp. 144–167, 2021.

[15] Q. Wu and R. Zhang, "Towards smart and reconfigurable environment: Intelligent reflecting surface aided wireless network," *IEEE Commun. Mag.*, vol. 58, no. 1, pp. 106–112, 2020.

[16] Z. Yang, W. Xu, C. Huang, J. Shi, and M. Shikh-Bahaei, "Beamforming design for multiuser transmission through reconfigurable intelligent surface," *IEEE Trans. Commun.*, vol. 69, no. 1, pp. 589–601, 2021.

[17] Z. Zhang and L. Dai, "A joint precoding framework for wideband reconfigurable intelligent surface-aided cell-free network," *IEEE Trans. Signal Process.*, vol. 69, pp. 4085–4101, 2021.

[18] L. You, J. Xiong, D. W. K. Ng, C. Yuen, W. Wang, and X. Gao, "Energy efficiency and spectral efficiency tradeoff in RIS-aided multiuser MIMO uplink transmission," *IEEE Trans. Signal Process.*, vol. 69, pp. 1407–1421, 2021.

[19] L. Dong, H.-M. Wang, and H. Xiao, "Secure cognitive radio communication via intelligent reflecting surface," *IEEE Trans. Commun.*, vol. 69, no. 7, pp. 4678–4690, 2021.

[20] X. Yu, D. Xu, Y. Sun, D. W. K. Ng, and R. Schober, "Robust and secure wireless communications via intelligent reflecting surfaces," *IEEE J. Sel. Areas Commun.*, vol. 38, no. 11, pp. 2637–2652, 2020.

[21] Y. Sun, K. An, J. Luo, Y. Zhu, G. Zheng, and S. Chatzinotas, "Intelligent reflecting surface enhanced secure transmission against both jamming and eavesdropping attacks," *IEEE Trans. Veh. Technol.*, vol. 70, no. 10, pp. 11 017–11 022, 2021.

[22] K. Liu and L. Dai, "Compact user-side reconfigurable intelligent surfaces for uplink transmission," *arXiv preprint arXiv:2107.08698*, 2021.

[23] Z. Lin, M. Lin, B. Champagne, W.-P. Zhu, and N. Al-Dhahir, "Secrecy-energy efficient hybrid beamforming for satellite-terrestrial integrated networks," *IEEE Trans. Commun.*, vol. 69, no. 9, pp. 6345–6360, 2021.

[24] E. Basar, M. Di Renzo, J. De Rosny, M. Debbah, M. Alouini, and R. Zhang, "Wireless communications through reconfigurable intelligent surfaces," *IEEE Access*, vol. 7, pp. 116 753–116 773, 2019.

[25] J. Dai, W. Tang, J. Zhao, and X. Li, "Wireless communications through a simplified architecture based on timedomain digital coding metasurface," *Adv. Mater. Technol.*, vol. 4, no. 7, pp. 1 900 044–1 900 044, 2019.

[26] C. Hu, L. Dai, T. Mir, Z. Gao, and J. Fang, "Super-resolution channel estimation for mmwave massive MIMO with hybrid precoding," *IEEE Trans. Veh. Technol.*, vol. 67, no. 9, pp. 8954–8958, 2018.

[27] G. T. de Arajo and A. L. F. de Almeida, "PARAFAC-based channel estimation for intelligent reflective surface assisted MIMO system," in *2020 IEEE SAM*, 2020, pp. 1–5.

[28] Y. Jiang, Y. Zou, J. Ouyang, and J. Zhu, "Secrecy energy efficiency optimization for artificial noise aided physical-layer security in OFDM-based cognitive radio networks," *IEEE Trans. Veh. Technol.*, vol. 67, no. 12, pp. 11 858–11 872, 2018.

[29] R. Schmidt, "Multiple emitter location and signal parameter estimation," *IEEE Trans. Antennas Propag.*, vol. 34, no. 3, pp. 276–280, 1986.

[30] W. Shi and J. Ritcey, "Robust beamforming for MISO wiretap channel by optimizing the worst-case secrecy capacity," in *2010 IEEE ACSSC*, 2010, pp. 300–304.

[31] *Maximum Allowable Values of Interference From Terrestrial Radio Links to Systems in the Fixed-Satellite Service Employing 8-bit PCM Encoded Telephony and Sharing the Same Frequency Bands*, document ITU-R SF.558-2, Jul. 1986.

[32] A. Beck, A. Ben-Tal, and L. Tetruashvili, "A sequential parametric convex approximation method with applications to nonconvex truss topology design problems," *J. Global Optim.*, vol. 47, no. 1, pp. 29–51, 2010.

[33] H. M. Al-Obiedollah, K. Cumanan, J. Thiyagalingam, A. G. Burr, Z. Ding, and O. A. Dobre, "Energy efficient beamforming design for MISO non-orthogonal multiple access systems," *IEEE Trans. Commun.*, vol. 67, no. 6, pp. 4117–4131, 2019.

[34] T. Lv, H. Gao, R. Cao, and J. Zhou, "Co-ordinated secure beamforming in K-user interference channel with multiple eavesdroppers," *IEEE Wireless Commun. Lett.*, vol. 5, no. 2, pp. 212–215, 2016.

[35] C. Wang, H.-M. Wang, D. W. K. Ng, X.-G. Xia, and C. Liu, "Joint beamforming and power allocation for secrecy in peer-to-peer relay networks," *IEEE Trans. Wireless Commun.*, vol. 14, no. 6, pp. 3280–3293, 2015.

[36] L. Liu, R. Zhang, and K.-C. Chua, "Achieving global optimality for weighted sum-rate maximization in the K-user gaussian interference channel with multiple antennas," *IEEE Trans. Wireless Commun.*, vol. 11, no. 5, pp. 1933–1945, 2012.

[37] T. Lipp and S. Boyd, "Variations and extension of the convexconcave procedure," *Optimization Engineering*, vol. 17, no. 2, pp. 263–287, 2016.

[38] S. Boyd and L. Vandenberghe, *Convex Optimization. Cambridge, U.K.: Cambridge Univ. Press*, 2004.

[39] S. Verdu and H. Poor, "On minimax robustness: A general approach and applications," *IEEE Trans. Inf. Theory*, vol. 30, no. 2, pp. 328–340, 1984.